Resistive-Pulse Sensing—From Microbes to Molecules

Hagan Bayley[†] and Charles R. Martin*[,‡]

Department of Medical Biochemistry and Genetics, Texas A&M University System Health Science Center, 440 Reynolds Medical Building, College Station, Texas 77843-1114, Department of Chemistry, Texas A&M University, College Station, Texas 77843-3255, and Department of Chemistry and Center for Research at the Bio/Nano Interface, University of Florida, Gainesville, Florida 32605-1200

Received October 19, 1999

Contents

I. Introduction

In this review we bring together and discuss a number of different manifestations of a chemical-sensing paradigm sometimes called the resistive-pulse method. In the simplest terms, this method is based on an electrochemical cell in which a small aperture separates two ionically conductive salt solutions. An electrode is placed into each salt solution, and an ionic current is passed through the aperture. An analyte species whose diameter is comparable to the inside diameter of the aperture is then introduced into one of the salt solutions. As we shall see here, depending on the size of the aperture, the analyte might be a microbe or a molecule or have dimensions anywhere in between. When the analyte enters the aperture it partially occludes the pathway for ionic conduction and the ionic current through the aperture decreases. Depending on the device, this change in current (or in some devices potential required to maintain a constant current) can be used to size, identify, and determine the concentration of the analyte species.

The classical example of a resistive-pulse sensor is the Coulter counter, a commercially available device used to count and size biological cells and colloidal particles. This device is reviewed briefly here as are some more recent experimental Coulter-type devices that make use of smaller apertures and thus can count smaller particles. We then turn our attention to the interesting and challenging problem of resistive-pulse sensing of molecules and ions rather than microbes or colloidal particles. Molecule and ion sensing is possible if the aperture used in the sensing element is of molecular dimensions. This review focuses on sensors containing molecule-sized apertures borrowed from Mother Nature—protein channels and pores—and on synthetic analogues of such nanoscopically sized channels.

Prototype sensing devices based on a number of different types of biological channel systems, including α-hemolysin channels, acetylcholine receptors, other ligand-gated channels, and K^+ channels, will be reviewed here. Emphasis will be placed on devices that use a single channel (typically an α-hemolysin channel) as the sensing element. As we shall see, these devices can detect individual analyte/channel interactions and convert these stochastic events into a current pulse train that contains information about both analyte identity and concentration. The power of protein engineering to tailor these channels for particular sensing applications is also discussed and demonstrated.

Synthetic analogues of these naturally occurring nanoscopic channels have recently been prepared and used in a prototype device for molecule and ion

[†] Texas A&M University System Health Science Center and Texas A&M University.
[‡] University of Florida.
* To whom correspondence should be addressed. Phone: 352-392-8205. E-mail: crmartin@chem.ufl.edu.

10.1021/cr980099g CCC: $35.00
Published on Web 06/21/2000

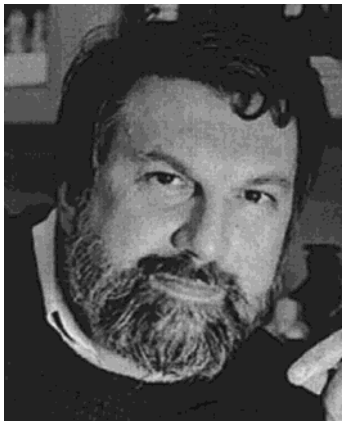

Hagan Bayley is Professor and Head in the Department of Medical Biochemistry & Genetics at Texas A&M University, where he also a Professor of Chemistry. He enjoys working at the interface of chemistry and biology by, for example, developing techniques for protein modification that have applications in both basic science and biotechnology. He received his B.A. in chemistry from the University of Oxford in 1974, while at Balliol College, and his Ph.D. in chemistry from Harvard University in 1979 in the laboratory of Jeremy Knowles. After postdoctoral work with Gobin Khorana at the Massachusetts Institute of Technology, he was on the faculty at Columbia University and the University of Oxford. From 1988 to 1996, he was at the Worcester Foundation for Experimental Biology in Shrewsbury, Massachusetts.

Charles R. Martin is Professor of Chemistry and Director of the Center for Research at the Bio/Nano Interface at the University of Florida. His research Interests lie at the interfaces between analytical chemistry, electrochemistry and materials science. Areas of special interest include nanomaterials and nanoporous membranes for chemical and bioseparations and analyses, molecular-recognition membranes, electrochemistry of nanoscopic electrodes and materials, and electrochemical energy storage and production. He received his B.S. degree at the Centre College of Kentucky. He did graduate work at the University of Arizona with Henry Freiser and postdoctoral work at the University of Texas with Allen Bard. He started his academic career at Texas A&M University in 1981, moved to Colorado State University in 1990, and then to the University of Florida in 1999.

sensing. These synthetic nanotubules are composed of gold and are prepared by electroless deposition of Au within the pores of a commercially available microporous filtration membrane. This process yields a robust sensor membrane that contains a collection of monodisperse Au nanotubules with inside diameters of molecular dimensions that span the complete thickness of the membrane. These Au nanotubule membranes can be used to detect molecules and ions at concentrations as low as 10^{-11} M. In principle, stochastic sensing should also be possible with these synthetic nanotubules.

II. Resistive-Pulse Detection of Cells and Small Particles

A. The Coulter Counter

The Coulter counter (Beckman Coulter, Fullerton, CA) is a device used to count and size biological cells, microorganisms, and other small particles.[1−4] Because so much information on this device is available from Beckman Coulter[3] and its competitors[4] and because there are many authoritative reviews of this subject,[1,2] the discussion here will be brief.

In the Coulter counter, a small diameter aperture (from ~20 μm to as large as 2 mm) separates two electrolyte solutions and a constant ionic current is passed through this aperture. The aperture is typically bored through a man-made sapphire, the thickness of which is comparable to the diameter of the aperture.[5] The sapphire is then heat sealed into a glass tube called the aperture tube. A variety of aperture sizes is available with each instrument. An electrolyte solution is placed within the aperture tube, and the tube is immersed into a solution of the same electrolyte. The electrolyte solution surrounding the aperture tube contains the suspended biological cells (or other particles) to be counted, and this solution is forced to flow through the aperture. Flow is driven by a pressure gradient across the aperture, and with modern instruments, the volume of liquid sampled can be precisely controlled.[3]

When a particle enters the aperture it effectively displaces a volume element of electrolyte solution equivalent to the particle volume. As a result, the aperture resistance increases during the residence time of the particle in the aperture. This transient increase in aperture resistance is monitored via the corresponding increase in transaperture voltage drop. The number of such voltage pulses provides a count of the particles suspended in the electrolyte. The height of the pulse is proportional to the volume of the particle in the aperture, so particle size information can also be obtained. Indeed, the distribution of pulse amplitudes reflects the relative distribution of the volumes of the particles counted.[2] Several thousand particles per second can be sized in this way.

Commercial instruments can measure particles with diameters ranging from as small as ~400 nm to as large as ~1 mm.[1−4] The diameter of the particle to be counted determines the diameter of the aperture used in the instrument. As would be expected, the smaller the particles to be counted, the smaller the aperture used. Any given aperture can detect a range in particle sizes. For example, Lines states that a 30 μm aperture will measure particles ranging from 500 nm to 20 μm.[1] This is in agreement with the Beckman Coulter product literature, which states that an aperture can be used to detect particles in the range from 2% to 60% of the aperture diameter.[3] The lower size limit for a given aperture is determined by the electrical noise associated with the passage of the ionic current through the aperture; i.e., when the magnitude of the voltage pulse is equivalent to the noise level, detection becomes impossible. The size upper limit is determined by the ability to keep the particle in suspension.

The Coulter counter has been used routinely for 40 years to size and count numerous types of microorganisms and other particles including blood cells (both red and white), spermatozoa, platelets, tissue culture cells, algae, suspensions, slurries, yeasts, etc.[3] Some very recent examples of the use of the Coulter counter include applications in the wars against AIDS[6] and cancer.[7] For example, the Coulter counter was used to generate hematological parameters in pregnant women in a study of mother-to-child transmission of HIV[6] and in studies of the effect of insulin-like growth factors on oestrone sulfatase activity in human breast cancer cell lines.[7]

B. Other Coulter-Type Resistive-Pulse Detectors

Since the diameter of the particle that can be detected is determined by the diameter of the aperture used, it is obvious that to detect smaller particles, smaller apertures must be obtained. DeBlois and Bean described a Coulter-type device that used a 500 nm diameter pore in a track-etched polycarbonate membrane as the aperture.[8,9] Because of the smaller aperture, this device could detect particles with diameters as small as 60 nm. For example, virus particles were detected with this device.[9]

Because track-etched membranes will be featured heavily in the final section of this review, this process is reviewed briefly here. The track-etch process[10] entails bombarding a solid material (in this case a 10 μm thick polycarbonate film) with a collimated beam of high-energy nuclear fission fragments to create parallel damage tracks in the film. The damage tracks are then etched into monodisperse cylindrical pores by exposing the film to a concentrated solution of aqueous base. Such track-etched polycarbonate (and polyester) films are sold commercially as filtration membranes (e.g., Nuclepore, SPI-Pore, Poretics, Osmonics). Membranes with pore diameters ranging from as small as 10 nm to as large as 12 μm are commercially available.

The diameter of the pores is determined by the etch time and the etch-solution temperature. The density of pores is determined by the exposure time to the fission-fragment beam. Commercially available filtration membranes of this type have pore densities as high as 6×10^8 pores per cm^2 of membrane surface area. This makes the average distance between pores very small, on the order of 200 nm. In contrast, DeBlois and Bean prepared membranes with only 5×10^3 pores cm^{-2}, with an average distance between pores of $\sim$70 μm. With such lower pore-density membranes, they were able to identify a single pore using a light microscope. The surrounding pores were then masked with epoxy. This piece of membrane with the isolated single pore was used as the aperture in the Coulter-type device.

Li and Crooks recently described an experimental Coulter-type device where a glass fiber imbedded in a gold film was used as the template to form the sensing aperture.[11] The glass fiber was essentially "potted" into the Au film by electrochemical deposition of the Au around the fiber. The fiber was then dissolved away to yield an aperture that was $\sim$1.5 μm in diameter and $\sim$6 μm long. The authors present preliminary data showing that this device can be used to count 440 nm diameter polystyrene spheres. They also discuss the possibility of scaling this process down to make stochastic molecule sensors but admit that the technological challenges would be difficult. Finally, there have been recent attempts to micromachine Coulter-type devices (see ref 12 and references therein).

III. Using Biological Channels for Sensing

With this brief introduction to the concept of resistive-pulse sensing, we turn our attention to the interesting and challenging idea of detecting molecules and ions via this general approach. This requires molecule-sized apertures, and in this section we discuss apertures borrowed from Mother Nature. We first review the enabling concept of single-channel current recording as a way of monitoring channel activity and the interaction of channel blockers with the channel. We then discuss the analogy between blocking of a protein channel by a molecular or ionic species and blocking of the Coulter aperture by a particle. The characterization of polymers with protein channels is reviewed, including the exciting prospect of DNA sequencing with such channel-based detectors. Stochastic sensing with engineered α-hemolysin channels is then discussed.

A. Single-Channel Recording

Techniques for detecting the movement or activity of single protein molecules are under intense development, particularly those that employ improved optical approaches and new procedures for force measurement.[13−15] While this area is of great current interest, it is important to point out that single-channel current recording was achieved 30 years ago. At that time, there was already considerable support for the existence of ion channel proteins, based on a variety of indirect evidence.[16] The development of planar bilayer recording[17] opened up the possibility of single-channel current measurement, which was first achieved with an identified molecule by Hladky and Haydon, who observed the opening and closing of individual channels formed by gramacidin A, a peptide antibiotic[18] (Figure 1). In earlier work, increasingly convincing evidence for single channels had been obtained with EIM (excitability inducing material), a bacterial extract.[19,20]

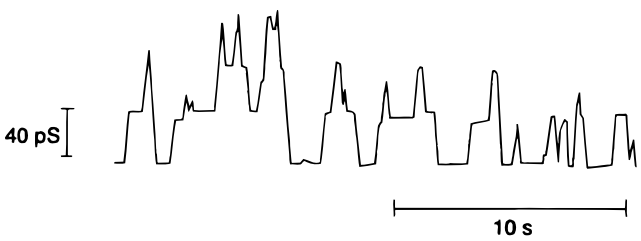

Figure 1. Current trace from the paper by Hladky and Haydon[18] describing the first definitive single-channel recordings from a bilayer of glycerol mono-oleate containing a low concentration of gramicidin A. The aqueous phase contained 1 M KCl. Channel openings are upward deflections.

During the same period, several estimates of single-channel conductance and the kinetics of channel blockers were obtained by the analysis of macroscopic current fluctuations.[21,22] In the 1970s, patch clamp technology developed by Neher and Sakmann,[23] and later improved with high-resistance (gigaohm) seals,[24] allowed single-channel recording from intact biological membranes. These advances have led to additional configurations for reconstituting purified channel proteins such as tip-dip recording, where a bilayer is formed on a patch pipet. This minimizes the capacitive current associated with the larger area of a conventional planar bilayer and thereby improves time resolution and signal-to-noise.[25,26] However, from an experimental point of view (as exemplified by the work on α-hemolysin, below), conventional bilayer recording, in which a bilayer is formed in a partition separating two compartments,[27] has the considerable advantage of providing access to both sides of the membrane (cis and trans) and, therefore, both entrances of a channel or pore after vectorial insertion or assembly into the membrane.

B. Channel Block in Ion Channel Proteins: Comparison with the Coulter Counter Concept

Rapid ion flux across biological membranes, notably in neurons, is mediated by ligand- and voltage-gated ion channels.[16,28−30] A second class of transmembrane proteins are pores, which are larger in diameter and epitomized by several bacterial toxins[31] and outer membranes proteins (e.g., the porins).[32−34] Here, for simplicity, we refer to both channels and pores as channels and the conductive pathway as the channel lumen.

Channel activity can be modulated by several classes of agents. One large class comprises channel blockers, which can be natural in origin and endogenous to the tissue in which the channel is located (e.g. cytoplasmic polyamines and Mg^{2+}, which act on many eukaryotic channels), natural but exogenous (e.g. plant and animal toxins), or synthetic (e.g. various therapeutic agents). Channels can exist in closed and open states, and a channel blocker reduces (partial block) or eliminates (full block) the conductance of an open state. Some natural channels have built-in blocker domains, such as the N terminus (ball) of Na channels[29,35] and the C terminus of certain porins.[36−38]

At the single-channel level, blocking events at the intermediate time scale can be observed as a modulation of the single-channel current. Here, the residence time of the blocker is shorter than the lifetime of the open channel but longer than the 100 μs that can be readily resolved by current recording (Figure 2). This modulated current has a high information content. In particular, the modulated current reveals both the identity and concentration of a blocker, allowing a channel protein to be used as stochastic sensor element. The identity of the blocker is provided by the nature of the blocking events, e.g., the dwell time, the extent of block, and their voltage dependences.[16,39] The concentration is a function of the frequency of occurrence of the blocking events. By contrast, slow and fast block are less informative; slow block produces a prolonged loss of or reduction in single-channel current, while fast block produces a continuous reduction in the apparent conductance (with increased single-channel noise) (Figure 2).

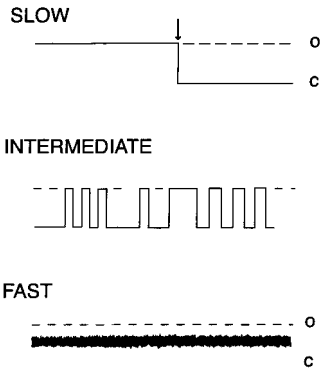

Figure 2. Fast, intermediate, and slow block at the single-channel level (schematic): o, open channel current; c, channel closed. Slow: The arrow marks a binding event. The current goes to zero and remains there for seconds to hours depending on the dwell time of the blocker. Intermediate: Rapid association and dissociation of the blocker give discrete events on the millisecond time scale. Fast: Blocking events on the microsecond time scale are too fast to record. The single-channel conductance appears to be lowered and excess noise is observed.

Figure 3. Early example of intermediate time scale block by an organic molecule.[40] The recordings showing single openings of the acetylcholine receptor in the presence of a local anesthetic, 10 μM QX-222. The downward events are the openings and the flickering within each event are QX-222 blockades.

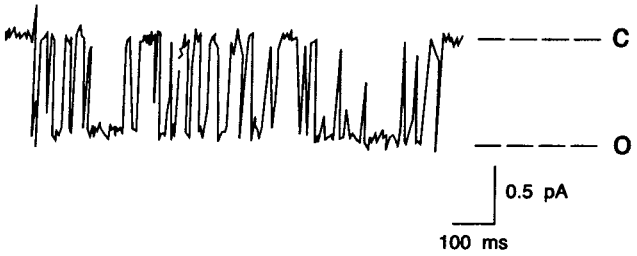

Figure 4. Early example of intermediate time scale block by a metal ion.[41] The recording is from a single open inwardly rectifying potassium channel in the presence of 10 μM Cs^+. The upward events are Cs^+ blockades.

Stochastic blocking of a single channel at the intermediate time scale was first observed by Neher and Steinbach,[40] who examined the interaction of the local anesthetic QX-222 with the acetylcholine receptor (Figure 3). QX-222 binds deep inside the channel lumen, as shown by the voltage dependence of block. Stochastic metal ion block, which is described later for engineered channels, was first observed as the voltage-dependent action of Cs^+ on single inward rectifier potassium channels[41] (Figure 4).

The case of intermediate time scale block is similar to the Coulter phenomenon. However, a channel blocker does not necessarily pass through a channel

as a particle does in a Coulter counter; a blocker can bind and dissociate from the same side of the bilayer and, therefore, act only from that side. In another variation, some channel blockers act from both sides of a membrane but behave differently when applied to one side or the other. This can arise if different sites are accessible from each side of the bilayer or if a common site is used but k_{on} (the rate constant associated with the formation of the blocker/channel complex) differs according to the side of blocker application or is voltage-dependent, as it will be for a charged blocker.[16,39] An example of a blocker that binds to two different sites is tetraethylammonium ion, which interacts with many voltage-gated potassium channels.[42] In principle, similar effects might be seen in a Coulter counter with a sophisticated engineered aperture.

A second class of channel blockers, of potential importance in stochastic sensing but largely unexplored in this context, act at sites distant from the conductive pathway as allosteric effectors. Activators of ligand-gated channels have been detected in sensing devices, but as yet, this approach has hardly been explored at the single-channel level (see section III.E, below).

C. Characterization of Polymers with Protein Pores

In an application that is in many ways most analogous to the Coulter counter, protein pores have been used to detect and characterize polymers that produce channel block. This work originated in experiments with a complementary objective: the use of polymers to characterize channels and pores. For example, estimates of the polymer exclusion limit[43] and changes in access resistance due to the presence of polymer[44,45] have been used to provide rough estimates of the "diameters" of channels. The osmotic effects of excluded polymers have been used to estimate the free energy of conformational changes in channel proteins that involve alterations in internal volume.[46] The interactions of short oligosaccharide substrates with porins, which are responsible for their passive transport across membranes, have also been examined.[47−49]

In some cases, these studies used current noise analysis[50,51] to examine the interactions of polymers with single channels.[45] Single-channel noise analysis was used earlier to study the interactions of ions[52,53] and more recently to look at small molecules, such as ATP.[54] The experiments with polymers suggested that only one or two molecules were present in the channel lumen at any given moment and that it might be possible to learn as much about the polymers as the proteins,[55] certainly to count and identify them.

Flexible polymers differ from classical channel blockers in that they do not bind in distinct conformations at specific sites in the channel lumen. Nevertheless, even polymers that do not interact with the walls of the lumen dwell in the channel for many nanoseconds.[45,54] Diffusion within the channel is restricted as expected for a polymer within a tube.[45,55] In this case, the excess single-channel current noise

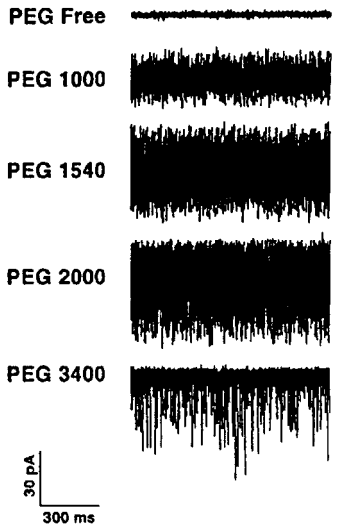

Figure 5. Current noise from a single α-hemolysin channel produced by poly(ethylene glycol)s of various molecular weights.[57] The aqueous phase was 1 M NaCl, 2.5 mM MES at pH 7.5 and contained PEG at 15% w/w.

is a function of the polymer mass and concentration as demonstrated for poly(ethylene glycol) (PEG) with the channel-forming peptide alamethicin.[45]

In another case, PEG and the α-hemolysin pore noise measurements suggest a weak, nonspecific interaction with the lumen wall producing greater excess noise and a sharper dependence on polymer mass than predicted for the absence of an interaction, peaking at 2000 Da[56,57] (Figure 5). The interaction is probably hydrophobic.[56,57] Indeed, the lumen wall of α-hemolysin contains hydrophobic belts, as do many other channels.[42,58,59] In other cases, more specific interactions may occur facilitating counting and identification. For example, oligosaccharides move through porins by guided diffusion on a "greasy slide" as visualized by X-ray crystallography.[48,59,60] Cyclodextrins, relatively rigid cyclic polymers, bind tightly at a specific site in the α-hemolysin channel with a dwell time of several milliseconds.[61]

It may be possible to engineer the interactions of polymers with channel walls to ease counting and identification, as suggested by experiments in which the interaction of PEG with α-hemolysin was controlled by pH.[57] Indeed, mutagenesis can increase the affinity of cyclodextrins for α-hemolysin by over 10^4-fold.[61] It must be added that single-channel noise analysis can be trickier than the interpretation of current modulation in the intermediate time scale (Figures 2−4) and the outcome is sometimes ambiguous.

D. Characterization of Nucleic Acids with Protein Pores

Building on the earlier observations with simple polymers such as PEG and dextrans, Kasianowicz and colleagues applied single-channel recording to the observation of single-polynucleotide (DNA and RNA) molecules.[62] The ultimate goal is DNA sequencing,[62−64] and while this may be far-fetched in the present formulation, the approach can already reveal some aspects of DNA or RNA composition. The

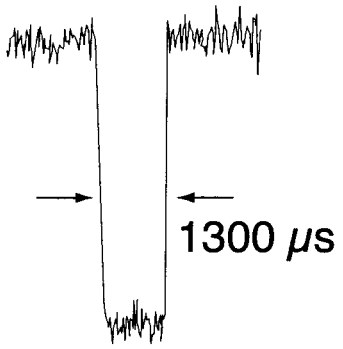

Figure 6. Polynucleotide block of a single α-hemolysin channel.[62] An example from the class of longer events is shown. The current through the open channel (120 pA in 1 M KCl) is almost completely blocked during the transit of a poly[U] molecule of 210 nucleotides.

molecules can be counted and their lengths determined. Limited information about base composition and distribution can be obtained.

At an applied transmembrane potential of 120 mV, single-stranded RNA molecules thread into the α-hemolysin pore and move through the lumen at 1 or 5 μs/base producing single-channel blocks of 85−100% of the unitary conductance[62] (Figure 6). The two transit times could represent 5′- and 3′-end threading. Occasional very long-lived blockades are seen that may be attributed to the entry of entangled structures or structures with secondary structure. Transient blockades representing "collisions" with the channel entrance were also noted. In the case of simple polymers such as PEG, it was not proven that the polymers actually pass all the way through the α-hemolysin channel. To produce single-channel noise, they would not have to, and there is a central constriction in the lumen of α-hemolysin that may prevent larger neutral polymers from passing in the majority of encounters. By contrast, the appearance of a single-stranded DNA in the opposite chamber of a bilayer apparatus was demonstrated by amplifying the translocated strands with the polymerase chain reaction.[62] This is analogous to the Coulter counter where complete transport of the blocking species through the aperture also occurs.

Unlike the brief interactions of PEG molecules small enough to enter the channel lumen, the transit times of long DNA molecules through the α-hemolysin pore are in the millisecond range and easily registered as individual current blockades. Provided that the necessary calibration is done, DNA molecules can be counted. If the base composition is known, the length of nucleic acid chains can be determined from the transit times, although a published transit time histogram shows rather broad peaks.[62] Conversely, a rough value for the base composition might be determined if the molecular mass were known.

With respect to DNA sequencing, at this point, only long stretches of a given nucleotide can be distinguished from long stretches of another within a single molecule.[64] This is not surprising given that at least 20 nucleotides will lie within the lumen of the α-hemolysin pore at any given time, and molecular modeling suggests that a large fraction of them would

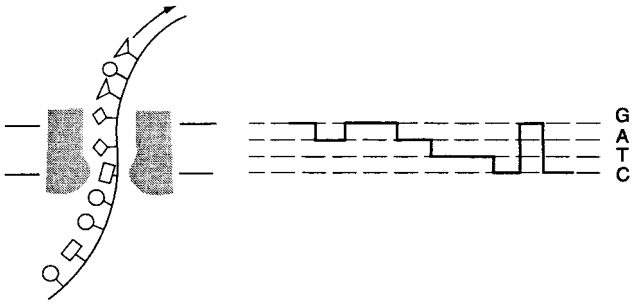

Figure 7. Concept for sequencing DNA by using a single protein pore.[64] A single-stranded DNA (or RNA) molecule moves through the pore in the transmembrane electric field. As it passes a "contact site", each base produces a characteristic modulation of the amplitude in the single-channel current.

contact the lumen wall. At present, there is no evidence that signals from individual bases can be distinguished by this approach (Figure 7). As the proponents of sequencing suggest,[62,63] several improvements must be made before the concept can be properly evaluated.

First, a limiting aperture or high-affinity contact site must be engineered into the channel lumen to provide base identification through either a characteristic extent of block or dwell time. The four dwell times (for G, A, T, and C) would each have to be separated by an order of magnitude, and even then the error rate would be high. Therefore, it might be best to seek four clearly separated extents of block (Figure 7), which might in turn require the replacement of one or more of the bases with a bulky or charged analog.[63] Second, the transit time per base must be increased into the measurable range. The contact site might serve this role, but other solutions are possible, for example, the use of polymerases to allow slow stepwise synthesis of a single-stranded polynucleotide from a double-stranded template for insertion and transport through the channel.[63] Third, any backward movement of the DNA strand would have to be reduced to an acceptable level of ∼1 in 1000 bases. This might be accomplished, for example, by adjusting the physical conditions (e.g., by using a high transmembrane potential), by altering the properties of the channel protein by mutagenesis or targeted modification, or by using the driving force of a polymerase. Finally, just as in the case of the development of chemical and enzymatic DNA sequencing, there will be a need to overcome problems associated with polynucleotide secondary structure.

Ultimately, implementation of DNA sequencing may require the use of new technologies such as nanoscopic pores made of inorganic materials[64] (see below). At the very least, further research in this area will lead to improved polymer characterization and a better understanding of how polymers pass through bilayers. Some very recent work in this regard is worth mentioning. For example, a theoretical explanation has been provided for the broad distribution of transit times of polynucleotides through the α-hemolysin pore.[65] A detailed description of the discrimination between poly A and poly C segments in a block has been published.[66] This paper is accompanied by a thoughtful commentary.[67] The

strong dependence of polynucleotide transit time on temperature has been documented.[68] Finally, the utility of polymers for the characterization of pores has been expanded with the demonstration that the simultaneous application of different polymers to each side of a pore can reveal the existence of internal constrictions.[69]

E. Additional Sensing Applications of Natural Ion Channels

To date, polymers have been characterized by using unmodified channel proteins. Natural proteins have also been used in other situations. Sniffer patches were devised to detect, with high spatial resolution, low levels of acetylcholine secreted by the growth cones of neurons.[70,71] The functional component of the first patches was the acetylcholine receptor (AchR), a ligand-gated ion channel. For example, outside-out patches containing up to 300 AchR were excised from cultured chick myotubes.[70] The responses of single channels could be readily observed. Indeed, the sniffer patch approach is so sensitive that it can be used to detect quantal (single vesicle) release of transmitters from nerve terminals.[72] In addition to acetylcholine, transmitters including ATP, glutamate, and γ-aminobutyric acid have been detected.[72]

A related approach, patch cramming, has been used to detect second messengers inside cells.[73] In this case, an inside-out patch carrying the channel acting as a sensor is forced through the membrane of the cell under examination (Figure 8). The activities of many eukaryotic channels are modulated by intracellular messengers and patches containing them can be taken from a variety of donor cells. Ions and molecules that have been detected in this way include Ca^{2+} [73] and cGMP.[74,75] To detect Ca^{2+}, a natural Ca^{2+}-activated K^+ channel was used. To detect cGMP, a mutant cyclic nucleotide-gated channel was used that was both highly selective for cGMP and highly sensitive (e.g., to as low as 0.5 μM cGMP). The altered protein was expressed at high levels in Xenopus oocytes, yielding patches with up to 1500 channels, permitting the observation of changes in intracellular cGMP in real time.[74,75] Single-channel responses were not examined in this work.

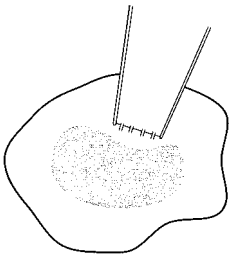

Figure 8. Patch cramming (schematic). A glass electrode containing responsive channels in a membrane patch is pushed into a recipient cell where it senses changes in intracellular second messenger concentrations.[68]

Zare and colleagues used intact two-electrode voltage-clamped Xenopus oocytes to detect molecules separated by capillary electrophoresis.[76] The oocytes were preinjected with mRNA encoding ligand-gated receptors for the analytes of interest. The idea was soon refined to incorporate patch-clamp recording.[77−81] For example, γ-aminobutyric acid, L-glutamate, and *N*-methyl-D-aspartate were distinguished by the responses of whole rat olfactory interneurons or outside-out patches from them, which contain several types of ligand-gated channel.[77,78,81] For whole cell recordings, mean single-channel conductances and corner frequencies (which yield analyte dwell times) were obtained from spectral analysis of current noise. These parameters were characteristic of various analyte−receptor combinations. Under favorable conditions, with outside-out patches, single-channel openings were observed.[77]

Future progress in this area will be expedited by the use of engineered channels, as initiated by Kramer and colleagues,[74] and by greater reliance on single-channel recording to take advantage of the additional information available with this mode of detection. In experimental biology, natural channels and simple mutants will continue to be useful, as the need is usually to detect natural products. For the detection of man-made analytes, more dramatic engineering of simpler proteins will be required (see below) and blocker sites as well as ligand activation should be exploited.

F. Engineered Channels

The use of unmodified membrane channels and pores as sensor elements has produced very promising results. However, the full promise of proteins in sensors lies in the modification of their properties by "protein engineering", a term that encompasses a multitude of manipulations and, as applied to membrane proteins, is in its infancy.[82] The possibilities include direct mutagenesis ("genetic engineering"), targeted chemical modification (both covalent and noncovalent), the incorporation of unnatural amino acids, and the manipulation of subunit composition.

Membrane proteins fall into two major classes: helix bundles and β barrels. As molecular modeling would suggest, the more open barrel structure is more amenable to extreme amino acid substitutions. For example, the entire transmembrane domain of α-hemolysin can be replaced by a barrel made from a reversed amino acid sequence.[83] It is unlikely that such a manipulation would work with a helix bundle in which amino acid side-chain interactions are important for structural stability.[84,85] The de novo design of channels is also producing promising results[82] but has not yet found applications in sensing. Combinatorial methods and directed evolution might too be combined with these approaches. No matter how they are produced, for applications in sensing it is desirable that engineered proteins undergo self-assembly and be readily reconstituted into lipid bilayers.

At present, the usual goal in engineering sensor elements is to produce new blocker sites within a channel. In stochastic sensing a completely selective binding site for an analyte is not required, as might be the case in a traditional immunoassay. This is because each analyte produces a distinctive signal associated with its binding kinetics (see below). Indeed, to do this, the analyte cannot bind too tightly,

which is one aspect of specificity. Allosteric sites, characteristic of ligand-gated channels (see section III.E), will be far harder to engineer from scratch and are not discussed here. In the following, engineered binding sites are described, exemplified by membrane proteins where possible.

Direct mutagenesis readily permits the incorporation of binding sites with relatively unsophisticated structural demands. For example, numerous cases of engineered binding sites for metal ions in a variety of proteins have appeared in the literature.[86,87] A site for Hg(II) or Ag(I) can be made simply by putting a cysteine residue in the desired place.[86−89] Sites for group IIb and various transition metal ions can be generated by replacing 2−4 natural residues with His, Glu, Asp, or Cys, often by using a combination of guesswork and simple-minded modeling[90−92] and occasionally by applying more sophisticated computational approaches.[86] The design of binding sites for analytes with more complex requirements than metal ions is far more difficult; success is usually achieved through modification of an existing site. For example, several general anesthetics act on the acetylcholine receptor as channel blockers. The sensitivity to a wide range of anesthetics is increased by mutations that introduce hydrophobic side chains into the channel lumen.[93,94]

Until molecular design has advanced, approaches based on the targeted modification of proteins are more likely to work for "complex" analytes. In general, targeted modification is achieved by covalent attachment at single cysteine residues. Most experiments with attached groups have again been done to introduce metal binding sites.[86,87,95] However, there are exceptions; for example, Schultz and colleagues appended single-stranded nucleotides near the active sites of nucleases to increase their specificity[96−99] and boronic acids can be attached to proteins for the capture of various sugar molecules.[100]

Molecules from the world of host−guest chemistry[101,102] might also be linked covalently to proteins to act as binding sites. Indeed, we showed recently that the *noncovalent* targeted modification of a protein pore can be used to create a blocker site. β-Cyclodextrin lodges at a specific site in the lumen of the α-hemolysin channel, where it binds a wide variety of organic molecules that in turn modulate current block[61] (see below). A variety of cyclodextrins can be used (ref 61 and unpublished work), and the protein can be tailored to accept them.[61] An additional means for modifying polypeptides is the introduction of unnatural amino acids by using preloaded tRNAs or by semisynthesis. Unnatural amino acid mutagenesis has been applied to the acetylcholine receptor by Lester, Dougherty, and colleagues,[103−108] in some cases to modify the channel lumen.[104,108]

Many membrane proteins are multimers, either homomeric or heteromeric, with the subunits grouped around a central molecular axis that lies perpendicular to the membrane surface. In the case of heteromers, questions arise concerning the stoichiometry of the subunits and their arrangement about the central axis. This engineering problem has been

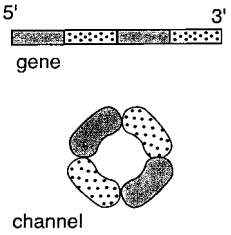

Figure 9. Subunit combinations and permutations in a multisubunit channel established with a genetic construct (schematic). Here a tetramer of the form $\alpha_2\beta_2$, with the subunits arranged alternately around the central axis, is made from a gene (top) in which the DNA encoding the four subunits is connected by short in-frame linkers. A view along the central axis of the channel is shown (bottom).

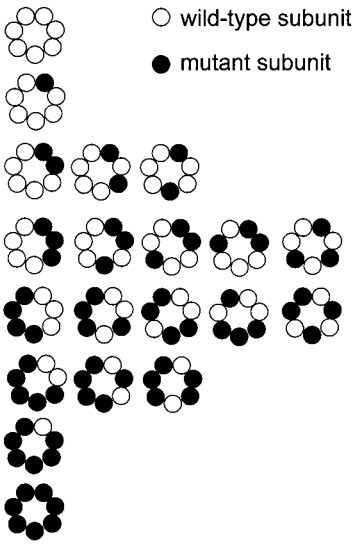

Figure 10. Subunit combinations in a multisubunit channel can be separated after targeted chemical modification (schematic). The example depicted is applicable to the staphylococcal α-hemolysin pore, which has seven subunits resulting in eight combinations of two types of subunit with 20 permutations in all. The combinations, shown in rows here, are readily separated by electrophoresis after selective modification of the mutant subunits with a charged reagent.[87]

solved in two ways. First, in favorable cases, the subunits can be chained together genetically (Figure 9). This is often done with eukaryotic channels in cases where the N and C termini of each subunit are found naturally on the same side of the bilayer, for example, with potassium channels.[109,110] This approach solves both the problem of subunit combination and that of permutation. In a second approach, the various subunit combinations are physically separated (Figure 10). For example, heteromeric α-hemolysin pores can be obtained by tagging mutant subunits on cysteine residues with charged reagents. The heteromers are then separated by electrophoresis.[92,111] At this time, heteromers with different permutations of subunits about the central axis have not been resolved by the second approach.

A variety of different procedures can be grouped under the heading of de novo design, and considerable progress has been made in this area.[82] Examples include channels built from α-helices, including noncovalent bundles[112−114] or bundles preorganized through template-assisted syntheses.[115−117] In addi-

tion, nanotubes have been built from cyclic peptides,[118] originally containing alternating D- and L-amino acids based on the gramicidin A sequence[119] but more recently containing β^3-peptide linkages.[120] Significant work has been done on size and charge selectivity with these structures, but so far blocker sites that would be required to make a sensor element have not been incorporated into de novo designed channel proteins. In several cases, the designed channels are not especially tolerant of blocker sites. For example, the helix bundles generally form rather narrow channels and the nanotubes have no inwardly directed amino acid side chains.

Additional approaches that might be applied to channel proteins include combinatorial methods and directed evolution. Coupled with powerful selection or screening tools, these approaches have been extremely powerful in the discovery of proteins that bind a variety of ligands, for example, the development of antibody-based enzymes (abzymes) selected with transition state analogues or by related means.[121−123] So far, the efficient selection or screening techniques that have been so effective in other circumstances have not been implemented to allow a search for channels with new blocker sites. Unexpected successes are likely to be uncovered when such searches are possible. For example, the examination of a small collection of α-hemolysins, mutated in the transmembrane domain, yielded pores with divalent metal [M(II)]-binding sites on the *outside* of the transmembrane β barrel.[124]

G. Detecting Small Molecules with Engineered Pores

In many ways staphylococcal α-hemolysin, which has been developed as a stochastic sensor element, is an exemplary target for protein engineering. α-Hemolysin is secreted by *Staphylococcus aureus* as a water-soluble, monomeric, 293-residue polypeptide which forms heptameric pores in lipid bilayers.[125,126] The pore is a mushroom-shaped structure in which the lower half of the stem, a 14-stranded β barrel, forms a transmembrane channel made up of residues from each of the central glycine-rich regions of the seven polypeptide chains[127] (Figure 11). The N- and C-terminal thirds of the polypeptides form the cap of the mushroom, which is also rich in β structure and resides outside the lipid bilayer. Transported molecules move through the 100 Å long water-filled channel lumen, which is centered on the molecular 7-fold axis (Figure 11). The α-hemolysin pore is

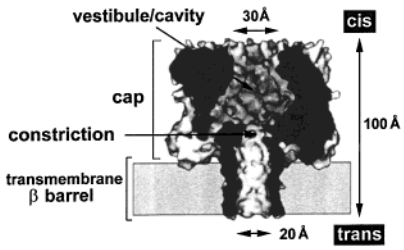

Figure 11. Essential features of the staphylococcal α-hemolysin pore shown in a sagittal section based on the crystal structure.[122] The cis and trans side of the bilayer as defined for planar bilayer recordings are indicated.

capable of transporting molecules of up to ~2000 Da across the membrane by passive diffusion.[128,129] Single-stranded nucleic acids of much larger mass, presumably in an extended form, can move through the central channel in a transmembrane electric field[62] (see above).

Several features of α-hemolysin have facilitated the investigation of engineered versions of the pore. Structures of the fully assembled α-hemolysin heptamer and of a related monomer (leukocidin F) have been solved by Eric Gouaux and colleagues.[127,130] The protein is robust; for example, the heptamer is stable in a denaturing detergent, sodium dodecyl sulfate, at up to 65 °C.[131] α-Hemolysin (αHL) and its mutants can be obtained in abundance by expression in either *S. aureus*[132] or *E. coli*,[133] and convenient for many purposes, small amounts are available by in vitro transcription and translation.[92,133]

The αHL pore efficiently self-assembles into lipid bilayers.[134] Assembly occurs with a defined subunit stoichiometry and in a single orientation with respect to the bilayer, by contrast with the multiple forms and dual orientation found in many other systems.[82] Heteromers of defined subunit composition can be prepared and incorporated into bilayers by direct insertion.[92] The protein is a blank slate in terms of protein engineering. For example, the high-conductance channel is more easily manipulated than a narrow channel. In addition, the wild-type channel remains open indefinitely at modest transmembrane potentials and is only weakly anion selective and weakly rectifying.[134] Finally, the αHL pore tolerates radical alterations in amino acid sequence.[83]

The potential of protein engineering has been demonstrated in two studies in which α-hemolysin was used first to detect divalent metal ions and second small organic molecules. Initially, divalent metal ions, M(II), were detected by examining macroscopic (many channel) currents through homomeric pores formed by αHL-H5.[135] This mutant contains five consecutive histidines in the transmembrane domain. H5 was made before the crystal structure of the pore was known, based only on the knowledge that the central region of the polypeptide chain became occluded during assembly and therefore perhaps entered the bilayer. Only subsequently could its properties be interpreted at the molecule level in the light of the structure.[127,130,136] M(II), such as Zn(II), prevent the formation of H5 pores[137] by locking the transmembrane sequences inside an assembly intermediate, the heptameric prepore.[130,136] After assembly in the absence of M(II), two of the five histidines in each subunit, 14 in all, project into the channel lumen.[127] M(II) cause complete single-channel block, not by a return to the prepore (the final step in assembly is irreversible), but most likely by causing the transmembrane barrel to collapse reversibly.

To allow stochastic sensing, a more subtle modulation of the single-channel current was sought, which required the introduction of a single mutant subunit into the heptamer: in other words, the formation and purification of heteromers of the form WT_6MUT_1, where WT is the natural, "wild-type" subunit and

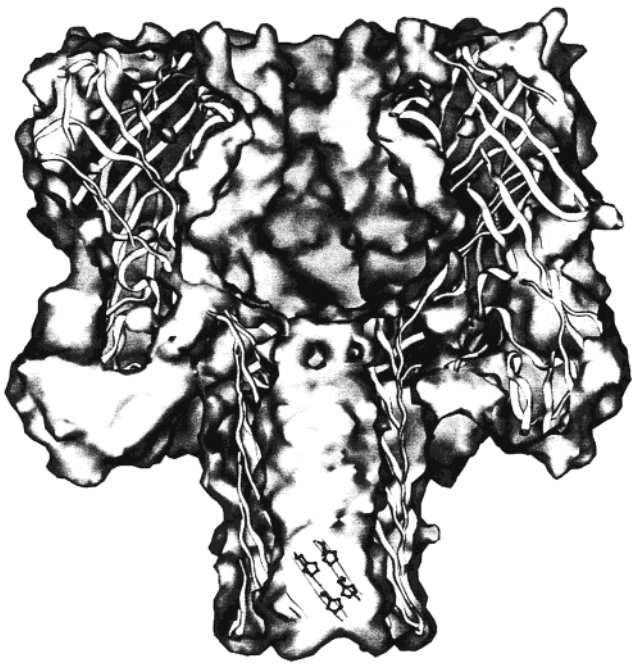

Figure 12. Sagittal section through the WT_64H_1 α-hemolysin pore.[87] The cutaway shows the M(II) binding site comprising four histidine side chains in the stem region that project into the lumen of the transmembrane channel.

MUT is the mutant subunit. The work was initiated with H5, but after the structure of the pore was revealed, it was completed with αHL-4H, a mutant containing four histidines all of which project into the channel lumen (Figure 12).[92] 4H also contained a single cysteine residue at position 292, far from the conductive pathway. Selective covalent modification at position 292 with a sulfhydryl-directed stilbene disulfonic acid permitted the separation of pores with different subunit combinations by SDS−polyacrylamide gel electrophoresis (see section III.F).

The resultant WT_64H_1 is an exemplary stochastic sensor element. In the absence of M(II), a steady single-channel current flows through a pore. In the presence of M(II), partial channel blocks are observed, which increase in frequency with M(II) concentration (Figure 13). While it seems likely on structural grounds that three rather than all four of the histidine residues coordinate M(II), the binding site is of high affinity, e.g., K_d Zn(II) = 110 nM. At Zn(II) concentrations of around K_d, the signal can be integrated over a few seconds to give a reliable estimate of concentration. Various M(II) (e.g., Co, Ni, Cu, Cd) give characteristic signals with WT_64H_1, allowing them to be distinguished.[92] The mutually exclusive site occupancy characteristic of the single-molecule approach allows two or more M(II) in solution to be identified and quantified simultaneously (O. Braha et al., unpublished data) (Figure 14). This is because each analyte metal ion produces a duration of current block that is characteristic for that metal ion. Since only a single metal ion can occupy the blocking site at any time, a pulse train consisting of individual pulses of duration characteristic of the metal ion occupying the site at that time is obtained. That is, an analyte solution containing two analyte ions would produce a pulse train composed of pulses of two durations, one characteristic of the first metal ion and one characteristic of the second. A detailed analysis of the binding kinetics has proved difficult for all the M(II) that can be detected, some of which produce complex bursts of binding events. Nevertheless, it can be shown that signals from mixtures are readily decomposed into the separate signals that would arise from the component ions of the solution. From there, it is a simple matter to determine the component M(II) concentrations (O. Braha and L.-Q. Gu, unpublished data).

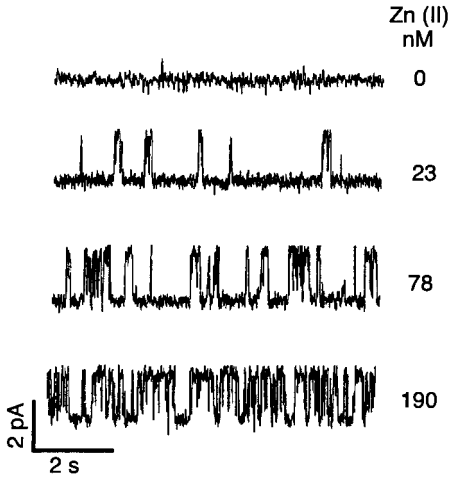

Figure 13. Detection of Zn(II) by the response of a single WT_64H_1 α-hemolysin pore. The single channel has a conductance of 660 pS (1 M NaCl, pH 7.5). The addition of buffered Zn(II) solutions produces transient blockades (upward events) of about 7% of the total current, which become more frequent with increasing free Zn(II) concentration.

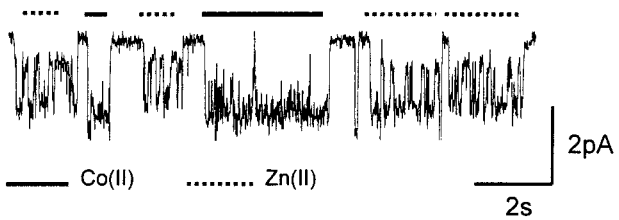

Figure 14. Assaying two analytes in a mixture by stochastic sensing with a single α-hemolysin pore. The response of a single WT_64H_1 pore to a mixture of Co(II) and Zn(II) is shown. The two ions cause distinct current fluctuations: Co(II), thick line; Zn(II), dashed line. The concentrations of the metal ions (Co(II), 10 μM; Zn(II), 120 nM) can be determined by analyzing the frequency of occurrence of the events.

WT_64H_1 is only one example of a heteromeric pore that can be generated from WT-αHL and 4H. While the others have not been examined in detail, we found that the affinity for M(II) and the complexity of the signals obtained from $WT_{7-n}4H_n$ both increased with n.[92] (The specific subunit permutations observed were not identified, although they are in effect separated in the single-channel experiments.) Clearly, many additional M(II)-binding subunits might be made by amino acid substitution in the β barrel or elsewhere in the channel. For example, M(II) sites have been placed on what is nominally the *outside* of the barrel and yield useful responses.[124] Hence, the approach is highly combinatorial with respect to

Figure 15. α-Hemolysin containing a β-cyclodextrin adapter responds to organic analytes. (Top) Sagittal section through the wild-type α-hemolysin showing the location of β-cyclodextrin when lodged in the lumen of the channel. (Bottom) Modulation of the single-channel current by a model analyte, 2-adamantanamine.[61] Level 1, open α-hemolysin pore; level 2, pore with bound β-cyclodextrin (20 μM, trans); level 3, pore with both bound β-cyclodextrin and bound 2-adamantanamine (80 μM, trans).

analytes (a single sensor element detects numerous M(II)), the nature and disposition of M(II) sites within individual mutant subunits generated by amino acid replacement, and the combinations and permutations of subunits that can be formed with them.

The demonstration of many of the predicted advantages of stochastic sensing with a pore containing blocker sites engineered for M(II) has encouraged the exploration of the same principle for sensing other analytes. The ability to examine small organic molecules is a challenge because they usually bind to proteins at largely preorganized sites that employ intricate stereochemistry to optimize hydrophobic, hydrogen bonding, and electrostatic interactions. Nevertheless, in the present case, relatively simple considerations might be used to build sites from amino acid side chains because for stochastic sensing, as emphasized earlier, binding sites need not be of extremely high affinity or specificity. So far, however, attempts to genetically engineer α-hemolysin to bind organics directly has met with marginal success. However, while this work has been underway, a different principle, that of the noncovalent molecular adapter, was discovered that should be of general applicability.

While seeking relatively rigid molecules for sizing pores, cyclodextrins were found to bind in the α-hemolysin channel and produce a substantial but incomplete channel block. Because cyclodextrins are well-known to bind small organic molecules in their hydrophobic interiors,[138] it was reasoned that organics might produce further block, and they did.[61] Stochastic sensing with cyclodextrin adapters was evaluated with a collection of adamantane derivatives whose interactions with cyclodextrins are well documented.[139] For example, the molecules gave distinctive blockades of the α-hemolysin·β-cyclodextrin complex (Figure 15).

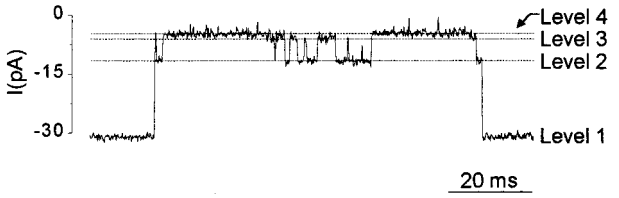

Figure 16. α-Hemolysin containing a β-cyclodextrin adapter can be used to detect two different organic analytes in a mixture. The experiment is the same as that depicted in Figure 15, with the addition of a second model analyte, adamantane-1-carboxylic acid (20 μM, trans). The latter produces longer blocks of greater amplitude (level 4) than 2-adamantanamine.

Figure 17. Adapters other than β-cyclodextrin can be used for stochastic sensing with α-hemolysin. The response of wild-type α-hemolysin to imipramine (100 μM) in the presence of γ-cyclodextrin (20 μM) is shown.

The kinetics of single-channel block were in keeping with a simple trimolecular scheme, involving one molecule each of the pore, β-cyclodextrin, and analyte, and the concentration of an analyte was readily determined from the concentration dependence of the signal. Further, as in the case of M(II) and $WT_6 4H_1$, different adamantanes produced characteristic signatures, as a consequence of their distinctive extents of block and dwell times (Figure 16). Again, this permitted two or more components of a mixture to be identified and quantified.[61]

Continuing work is establishing that a wide range of analytes, of far broader interest than the demonstration case of the adamantanes, can be examined by the adapter approach. For example, a variety of therapeutic drugs can be recognized and their concentrations determined.[61] Further, cyclodextrins other than β-cyclodextrin are effective and expand the range of signals that can be obtained and analytes that can be examined (Figure 17). Remarkably, αHL can be engineered to better secure the adapters. For example, homoheptameric pores formed from the mutant αHL-M113N bind β-cyclodextrin $\sim 10^4$ times more tightly than WT homoheptamers (L.-Q. Gu and S. Cheley, unpublished data). Again, stochastic sensing with protein pores is seen to be highly combinatorial, in this case with respect to analytes, adapters, and the proteins that accommodate them.

H. Practical Problems with Proteins

There is little doubt that improved protein sensor elements can be engineered.[82] In the coming years, new channel designs will be made based on structural information, which is beginning to emerge very rapidly for both α-helical transmembrane proteins[42,140] and those in the β barrel class.[33,36−38] Improved de novo design[141−143] and advancing techniques for targeted covalent[144] and noncovalent[61] modification will also impact membrane proteins. However, there

remains a need for enhanced screens for channels that are candidates as sensor elements and an improved ability to place channels in an environment more stable than conventional mechanically sensitive planar bilayers.

In terms of screening, the interactions of new channels with analytes or adapters might be determined quite rapidly in a flow device that presents a series of solutions to a channel in a bilayer at the end of an electrode made by a tip-dip procedure. For parallel screening of libraries of mutant channels, multiple single-channel recordings would have to be carried out simultaneously, and a system for doing this has not yet been built. Interestingly, very similar technology is required for sensor arrays or for sequencing numerous DNA strands simultaneously.

A more stable environment for channels would be provided by using solid supports, and steady progress is being made in this area.[145,146] In general, AC methods (e.g., impedance spectroscopy) are used to monitor channels in supported bilayers.[145,146] For these measurements, conducting supports are required which include noble metals (e.g., gold), inorganic oxides (e.g., indium−tin oxide), and conducting polymers. Recent studies have focused on producing supported bilayers with an aqueous layer between the bilayer and the support both to facilitate the incorporation of channels and to provide a reservoir of electrolyte that improves the electrical properties of the membrane.[146−148] Another important consideration has been to produce supported bilayers that are largely defect free, so that channels and not defects dominate the measurements.

Two groups have reported the switching of protein channels by using this technology.[149,150] In both cases, gold electrode surfaces were used and numerous active channels were present. For example, in one manifestation of their device, Cornell and colleagues used rather elaborate chemistry to place gramicidin channels in tethered supported bilayers. The lipids were anchored to the electrode surface by gold−thiol chemistry with a poly(ethylene glycol) spacer to provide a 40 Å aqueous layer between the surface and the bilayer. When an analyte, which can in this case be a small molecule, releases inactive half channels from an immune complex in the upper leaflet of the bilayer, they find half channels in the lower leaflet and form active open channels.[149] The impedance changes are reversed upon removal of the analyte.

Stora and colleagues placed the bacterial porin OmpF into a similar supported bilayer. They showed that the R fragment of the protein colicin N causes closures of the channels. Quantitative measurements in both papers suggest that either only a few of the membrane-inserted channels are functional[150] or their apparent conductances are lower than in conventional bilayers.[149] While these and related reports are promising, single-channel currents have not been recorded from supported bilayers. This is a requirement for stochastic sensing.

Given the limited progress with supported bilayers, unconventional approaches are worth examining. Schuster and collaborators recrystallized bacterial S layers on planar bilayers.[150] S layers are two-dimensional porous crystalline arrays of a single protein, which envelop many bacterial species. The S-layer-supported bilayers were able to incorporate active α-hemolysin pores and were more stable to rupture than conventional bilayers.[151,152] The gold nanotubule membranes discussed below might also be useful as supports of protein channels.

IV. Gold Nanotubule Membranes as Molecule and Ion Sensors and Molecular Filters

The concept of making membranes that contain a collection of monodisperse Au nanotubules that run the complete thickness of the membrane was introduced earlier. These Au nanotubule membranes are prepared using the "template method" where the cylindrical, monodisperse pores in a host membrane (or other solid) are used as templates to prepare nanomaterials.[153−163] This method has been used to prepare nanotubules, nanowires, and nanofibrils composed of a large variety of different materials including metals, semiconductors, other inorganic materials, carbons, polymers, etc.[153−163] As is the case for the Au nanotubules of interest here, the nanomaterials can be left imbedded in the pores of the template membrane. Alternatively, the template can be dissolved away and the liberated nanomaterials collected by filtration.

Commercially available polycarbonate filters prepared using the track-etch method (see above) are used as the templates for the Au nanotubule membranes. Filters with cylindrical 30 nm diameter pores, 6×10^9 pores/cm^2 of membrane surface area, are typically used.[154−157] An electroless plating method[160] is used to deposit the Au nanotubules within the pores (Figure 18A). Briefly, a catalyst is first applied to all surfaces (membrane faces plus pore walls) of the membrane. The membrane is then immersed into the electroless plating bath which contains a Au(I) species and a chemical reducing agent. Because the reduction of Au(I) to metallic Au only occurs in the presence of the catalyst, Au nanotubules that line the pore walls (Figure 18B) (as well as Au surface films on both faces of the membrane) are obtained.[153−157]

The thicknesses of both the surface films and the tubule walls increase with electroless plating time. As a result of the thickening of the tubule walls, the inside diameter (i.d.) of the tubules decreases with plating time. The i.d. is measured using a gas transport method described previously.[153−157,163,164] At long plating times, membranes containing tubules with i.d.s of molecular dimensions are obtained.[154] Finally, depending on the application, the Au surface films can be either left on the faces of the membrane or removed. For example, in the sensing application discussed below, the surface films were removed.

The template-prepared Au nanotubule membranes have been used as nonstochastic sensors for determination of ultratrace concentrations of ions and molecules.[156,157] Before discussing this sensor application, we review investigations aimed at understanding the basic transport properties of these new membranes.[154] These studies have shown that membranes containing nanotubules with i.d.s in the range

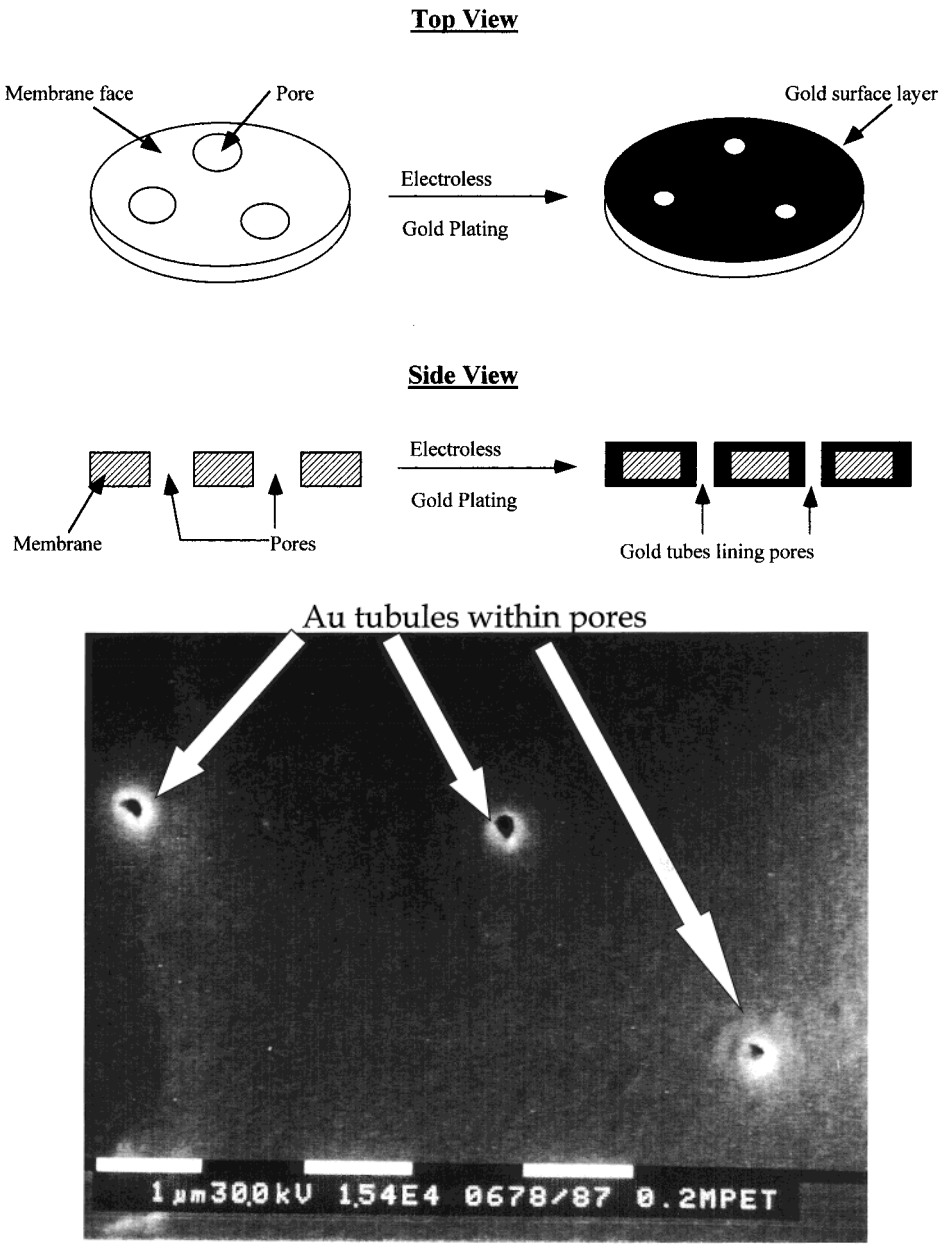

Figure 18. (A) Schematic of the electroless plating process used to prepare the Au nanotubule membranes. (B) Scanning electron micrograph (SEM) of the surface of a polycarbonate template membrane showing three Au nanotubules deposited within the pores. To visualize the tubules by SEM, the membrane had larger pores than those used to prepare the nanotubule membranes discussed here.

from ~2 to 5 nm can act as size-selective molecular sieves. Membranes containing nanotubules with i.d.s less than 1 nm can be used to cleanly separate small molecules on the basis of molecular sizes.

A. Transport Properties of the Au Nanotubule Membranes

1. Molecular-Sieving in Single-Component Permeation Experiments

These experiments were done in a simple U-tube permeation cell in which the nanotubule membrane separates a feed half cell from a permeate half cell. The feed half cell is charged with a solution of the molecule whose transport properties through the membrane are to be evaluated (often called the permeate molecule). The permeate half cell is initially water or a salt solution. Passive diffusion transports the permeate molecule from the feed half cell, through the nanotubule membrane, and into the permeate half cell. The permeate half cell is periodically assayed to determine the time dependence of transport of the permeate molecule through the membrane.

The transport data are processed as plots of moles of permeate transported vs time. Straight-line plots are obtained and the flux of the permeate molecule through the membrane is obtained from the slope. The experiment is then repeated using a solution of a second permeate molecule in the feed half cell. A membrane-transport selectivity coefficient (α) can then be obtained by ratioing the fluxes for the two permeate molecules. Since molecular-size-based se-

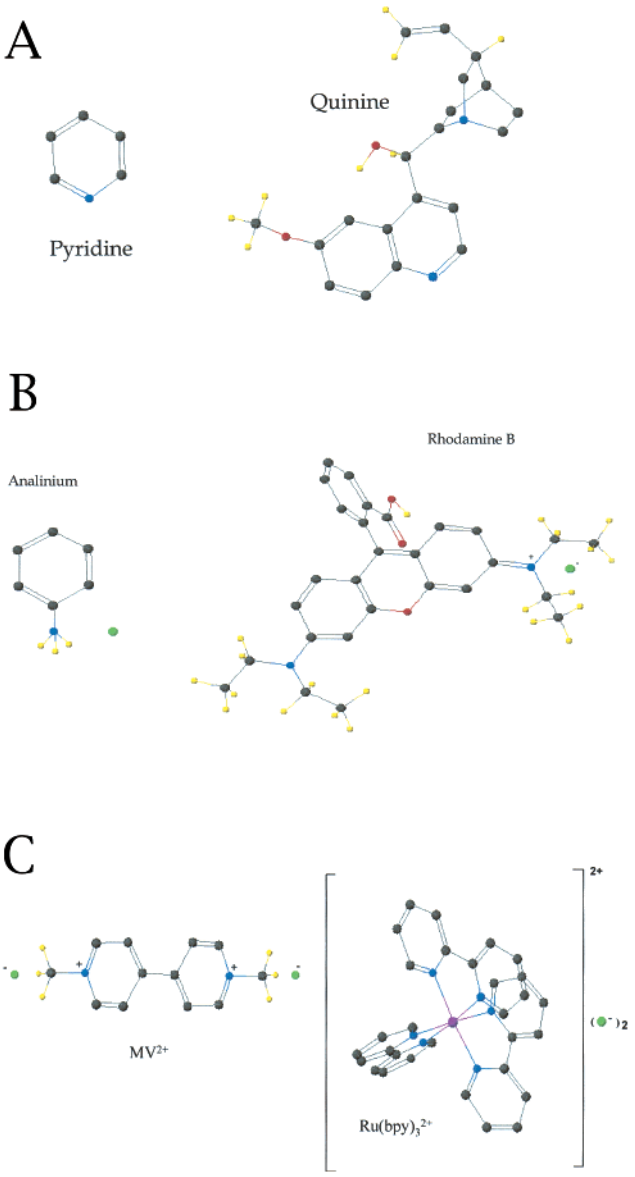

Figure 19. Chemical structures and approximate relative sizes of the three "big molecule/small molecule" pairs used in the molecular filtration experiments. Quinine, MV^{2+}, and $Ru(bpy)_3^{2+}$ were also used as analytes in the sensor work.

lectivity is of interest here, one of the permeate molecules was large—the tris-bipyridal complex of Ru(II), $(Ru(bpy)_3^{2+}$—and the other was smaller—methyl viologen, MV^{2+} (Figure 19).

The ratio of the diffusion coefficients for MV^{2+} and $Ru(bpy)_3^{2+}$ in free aqueous solution is 1.5.[165,166] For this reason, if a simple solution-like diffusion process were operative in the nanotubules, a selectivity coefficient of $\alpha = 1.5$ would be anticipated. In contrast, even for the largest i.d. nanotubules investigated (5.5 nm), the selectivity coefficient was substantially greater, $\alpha = 50$ (Figure 20A). These data suggest that size-based molecular sieving occurs in these large-i.d. (greater than molecular dimensions) nanotubules.[154,167,168]

Molecular-sieving is a result of hindered diffusion of the molecules in the Au nanotubules.[167] The simplest way to understand hindered diffusion is to consider first the Stokes−Einstein equation that

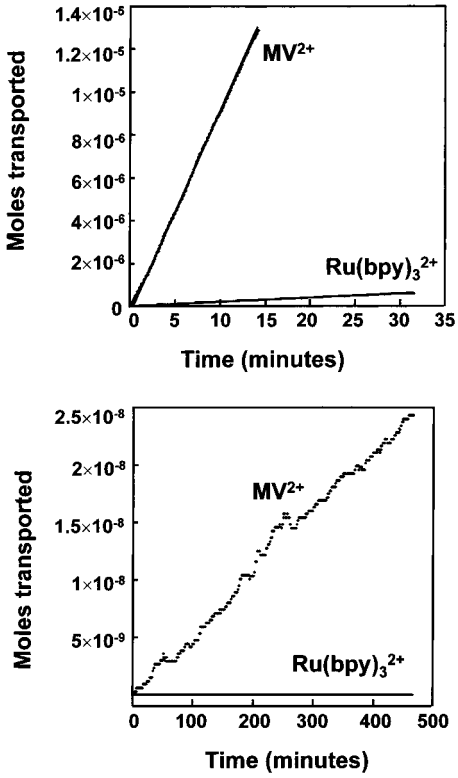

Figure 20. Single-molecule permeation experiments showing moles of MV^{2+} and $Ru(bpy)_3^{2+}$ transported versus time (see Figure 19C for chemical structures). Membranes contained nanotubules with i.d.s of (A) 5.5 and (B) ~0.6 nm. Only MV^{2+} was transported through this membrane (see ref 149 for details).

relates the diffusion coefficient (D_s) to molecular radius (r_m) for diffusion in free solution

$$D_s = kT/6\pi\eta r_m \qquad (1)$$

where k is the Boltzmann constant, T is the Kelvin temperature, and η is the viscosity. The denominator $6\pi\eta r$ can be thought of as a molecular-friction coefficient that determines the resistance to diffusion in the solution. As would be expected, this molecular-friction term increases with increasing size of the molecule and increasing viscosity of the solution.

In the Au nanotubule membranes, this molecular-friction coefficient is larger than in free solution because collisions with the nanotubule wall increase the frictional drag on the molecule.[168] In addition, diffusivity in the nanotubule is decreased, relative to a contacting solution phase, because of steric reasons.[167] Consider a molecule of radius r_{mol} diffusing within a nanotubule of comparable radius r_{tube}. Because the center of this molecule must always be a distance $\geq r_{mol}$ from the nanotubule wall, there are regions near the nanotubule wall that the molecule is sterically forbidden to occupy.[167−169] This makes the concentration of the molecule in the nanotubule less than the concentration in the contacting solution phase; put another way, the partition coefficient for the molecule into the nanotubule membrane is less than unity.[167] Since the flux is related to the concentration gradient in the nanotubule, this effectively lowers the nanotubule diffusivity.

The extent to which the diffusion coefficient for a molecule in the nanotubule (D_{tube}) is decreased rela-

tive to its value in free solution (D_{sol}) is related to the parameter λ, which is the ratio of the radius of the diffusing molecule to the radius of the nanotubule[167]

$$\lambda = r_{mol}/r_{tube} \quad (2)$$

A large number of theoretical expressions have been derived that predict how the ratio D_{tube}/D_{sol} varies with λ.[167−169] The extremes are easy to define; when $\lambda = 0$ ($r_{mol} \ll r_{tube}$), $D_{tube}/D_{sol} = 1$, and when λ approaches unity (tube and molecule are the same size), D_{tube}/D_{sol} must appraoch zero. The Renkin equation

$$D_{tube}/D_{sol} = 1 - 2.104\lambda + 2.09\,\lambda^3 - 0.95\,\lambda^5 \quad (3)$$

is an often-used example of the relationship between D_{tube}/D_{sol} and λ.[169] Plots of this equation and various other expressions for the relationship between D_{tube}/D_{sol} and λ can be found in the literature.[167−169]

Equations 2 and 3 show that for any i.d. nanotubule, diffusivity in the nanotubule membrane will be lower for the larger $Ru(bpy)_3^{2+}$ than for the smaller MV^{2+}. This is reflected in the transport data (Figure 20A) where the flux of the larger $Ru(bpy)_3^{2+}$ is decreased more than the flux for the smaller MV^{2+}. As a result, $\alpha = 50$ is obtained. Equations 2 and 3 predict that as the nanotubule i.d. is made smaller, the α value should become even larger, which is also reflected in the transport data. Values for 5.5, 3.2, and 2.0 nm i.d. nanotubule membranes are $\alpha = 50$, 88, and 172, respectively.[154] Similar sieving (but with lower selectivity) was observed in radiotracer self-diffusion experiments on lightly etched films prepared via the track-etch process.[170] However, molecular filtration of the type described below could not be observed.

2. Molecular Filtration in Two-Component Permeation Experiments

The smallest i.d. nanotubule membrane (i.d. ~0.6 nm) provides a measurable flux for MV^{2+}, but the larger $Ru(bpy)_3^{2+}$ could not be detected in the permeate solution, even after a 2 week permeation experiment (Figure 20B). These data suggest that clean separation (molecular filtration) of these two species should be possible with this nanotubule membrane. This was proven by doing two-molecule permeation experiments, where both the larger and smaller molecules (Figure 19) were present in the feed half cell together. A simple U-tube cell was used, and the permeate solution was periodically assayed, using UV−vis absorption or fluorescence, for both molecules. For all three of the large-molecule/small-molecule pairs shown in Figure 19, the small molecule could be easily detected in the permeate solution but the large molecule was undetectable.[154]

These data show that within the limits of measurement, the Au nanotubule membrane can cleanly separate large molecules from small molecules. However, one could argue that the large molecule is, indeed, present in the permeate solution but at a concentration just below the detection limit of the analytical method employed. This argument allows us to define a minimal transport selectivity coefficient (α_{min}) for each small-molecule/large-moleucle pair, where is α_{min} is defined as the measured concentration of the small molecule in the permeate solution divided by the detection limit for the large molecule. The α_{min} values obtained are extraordinary (Table 1). It is important to stress again that, in all three cases, the larger molecule was undetectable in the permeate solution. The value of α_{min} is simply determined by the ability to detect the larger molecule. Because rhodamine B can be detected to extremely low concentrations, α_{min} for this pair is the largest.

Table 1. Minimal Membrane-Transport Selectivity Coefficients

permeate pair	α_{min}
pyridine/quinine	15 000
anilinium/rhodamine B	130 000
$MV^{2+}/Ru(bpy)_3^{2+}$	1 500

Previous studies have demonstrated that these Au nanotubule membranes can show ionic charge-based transport selectivity and that the membranes can be electrochemically switched between anion transporting and cation transporting states.[153] Hence, these membranes can be viewed as universal ion exchangers. Furthermore, chemical transport selectivity can be introduced into these membranes by chemisorbing thiols to the inside tubule walls.[155,163] In this case, the chemisorbed thiol changes the chemical environment within the nanotubules and this, in turn, changes the transport properties of the membrane. For example, when the hydrophobic $HS-C_{16}H_{33}$ thiol is used, the membranes show high transport selectivity for hydrophobic permeate molecules.[163] Finally, it was shown here that these membranes can have molecular-size-based selectivity. Hence, these nanotubule membranes can utilize all of the selectivity paradigms (sterics, electrostatics, and chemical interactions) that Mother Nature uses in the design of Her exquisitely selective molecular-recognition schemes. For this reason, these membranes hold promise for the development of highly selective membranes for chemical separations and sensors.

B. Chemical Sensing with the Au Nanotubule Membranes

As in the resistive-pulse sensors reviewed here, the nanotubule membrane was allowed to separate two salt solutions, a constant transmembrane potential was applied, and the resulting transmembrane current was measured. When an analyte of comparable dimensions to the inside diameter of the nanotubules was added to one of the salt solutions, a decrease in transmembrane current is observed. The magnitude of this drop in transmembrane current (Δi) is proportional to the analyte concentration. However, because the patch of membrane used in this device contains numerous nanotubules, Δi is constant, i.e., not stochastic. As such, this device is similar to the protein-based systems, discussed above, where a large number of channels are incorporated into the sensing element.[70,74,75,135,149,150] Two important points are worth emphasizing. First, as defined here, the resistive-pulse umbrella covers both stochastic sen-

sors containing single channels or pores and devices that contain a number of pores, channels, or nanotubules. Second, by working with a piece of membrane that contains only a single pore, as DeBlois and Bean did in their device[8,9] (see above), stochastic sensing should be possible with the Au nanotubule membrane approach.

1. Calibration Curves and Detection Limits

As in the transport experiments, a U-tube cell was assembled with the nanotubule membrane separating the two halves of the cell. The two half cells were filled with the desired electrolyte, and an electrode was placed into each half cell. Three different sets of electrodes and electrolytes were used. The first set consisted of two Pt plate electrodes, and the electrolyte used in both half cells was 0.1 M KF. The second set consisted of two Ag/AgCl wires, and the electrolyte used in both half cells was 0.1 M KCl. The third set consisted of two Ag/AgI wires immersed in 0.1 M KI.

As noted above, the experimental protocol used with these cells was to immerse the electrodes into the appropriate electrolyte and apply a constant potential between the electrodes. The resulting transmembrane current was measured and recorded on an $X-t$ recorder. After obtaining this baseline current, the anode half cell was spiked with a known quantity of the desired analyte (Figure 19). This resulted in a change in the transmembrane current, Δi (Figure 21). A potentiostat was used to apply the

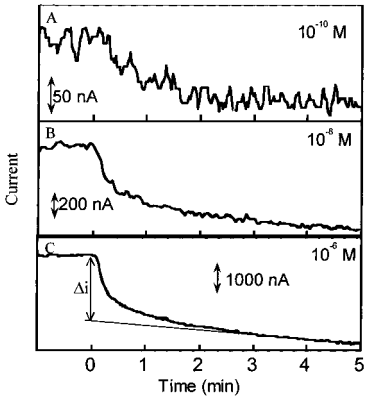

Figure 21. Nanotubule membrane sensor current−time transients associated with spiking the anode half cell with the indicated concentrations of $Ru(bpy)_3^{2+}$. Tubule i.d. = 2.8 nm; Ag/AgCl/KCl cell Δi determined as shown in C.

potential between the electrodes and measure the transmembrane current. The transmembrane potential used was on the order of 0.5 V.[156]

Plots of log Δi vs log[analyte] for the analytes $Ru(bpy)_3^{2+}$, MV^{2+}, and quinine (Figure 19) were obtained using Ag/AgCl electrodes and 0.1 M KCl as the electrolyte in both half-cells (Figure 22). A membrane with 2.8 nm i.d. Au nanotubules was used. A log−log format is used for these "calibration curves" because of the large dynamic range (spanning as much as 5 orders of magnitude in analyte concentration) obtained with this cell. Analogous calibration curves were obtained for the other electrode/electrolyte systems investigated. The detection limits[156]

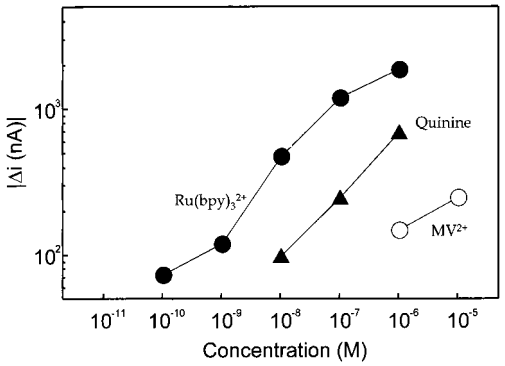

Figure 22. Calibrations curves for the indicated analytes. Membrane and cell as per Figure 21.

Table 2. Detection Limits Obtained for the Three Different Electrode/Electrolyte Systems Studied. Nanotubule i.d. = 2.8 nm

cell	analyte	detection limit (M)
Pt/KF	$Ru(bpy)_3^{2+}$	10^{-9}
Ag/AgCl/KCl	$Ru(bpy)_3^{2+}$	10^{-10}
	Quinine	10^{-8}
	MV^{2+}	10^{-6}
	2-naphthol	10^{-6}
Ag/AgI/KI	$Ru(bpy)_3^{2+}$	10^{-11}
	Quinine	10^{-8}
	MV^{2+}	10^{-7}
	2-naphthol	10^{-6}

obtained are shown in Table 2. For the divalent cationic electrolytes, the detection limits were lowest (best) in the Ag/AgI/KI cell and worst in the Pt/KF cell. The detection limit for quinine was the same in both the Ag/AgI/KI and Ag/AgCl/KCl cells. In general, the detection limit decreases as the size of the analyte molecule increases (see Figure 19). Finally, the detection limits obtained (down to 10^{-11} M) are extraordinary and compete with even the most sensitive of modern analytical methods.

The majority of the quinine in both the KCl and KI solutions is present as the monoprotonated (monocationic) form. Perhaps the reason the detection limits for $Ru(bpy)_3^{2+}$ and MV^{2+} are lower in the Ag/AgI/KI cell while the detection limit for quinine is the same in both this cell and the Ag/AgCl/KCl cell has to do with the difference in charge of these analytes (predominately monocationic vs dicationic). To explore this point, the detection limits for a neutral analyte, 2-naphthol, were obtained in both the Ag/AgI/KI and Ag/AgCl/KCl cells. Like quinine, the detection limit for this neutral analyte was the same in both cells (10^{-6} M, Table 2).

In the membrane transport studies it was shown that $Ru(bpy)_3^{2+}$ and MV^{2+} come across such membranes as the ion multiples $Ru(bpy)_3^{2+}(X^-)_2$ and $MV^{2+}(X^-)_2$ (X^- = anion).[154] In the KI cell, the ion multiple contains two larger (relative to chloride) iodide anions. Perhaps the larger size of the iodide ion multiple accounts for the lower detection limit in the KI-containing cell. If this is true, then the difference between the quinine cation paired with one I^- vs this cation paired with one Cl^- is not great enough to cause the detection limit for this predominately monovalent analyte to be significantly different in the Ag/AgI/KI vs the Ag/AgCl/KCl cells (Table 2).

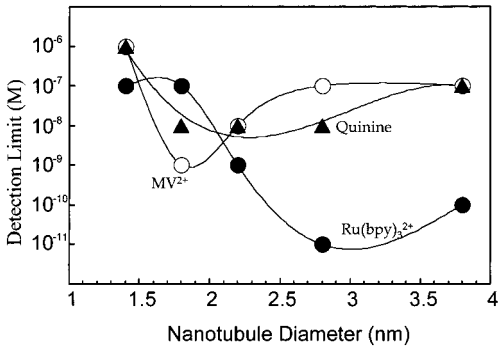

Figure 23. Detection limits for MV^{2+}, quinine, and $Ru(bpy)_3^{2+}$ vs i.d. of the nanotubules used in the sensor. Cell as per Figure 21.

The final variable to be investigated is the effect of nanotubule inside diameter on detection limit. To explore this parameter, membranes with nanotubule inside diameters of approximately of 3.8, 2.8, 2.2, 1.8, and 1.4 nm were prepared and used in the Ag/AgI/KI cell.[156] Calibration curves for the analytes $Ru(bpy)_3^{2+}$, MV^{2+}, and quinine were generated as before, and detection limits were obtained from these calibration curves. Figure 23 shows plots of detection limit for these three different analytes vs the nanotubule inside diameter in the membrane used. A minimum in this plot is observed for each of the three analytes.

The nanotubule membrane that produces this minimum (best) detection limit depends on the size of the analyte. These molecules decrease in size in the order $Ru(bpy)_3^{2+}$ > quinine > MV^{2+}. The nanotubule membrane that yields the lowest detection limit follows this size order; that is, the nanotubule diameters that produce the lowest detection limit for $Ru(bpy)_3^{2+}$, quinine, and MV^{2+} are 2.8, 2.2, and 1.8 nm, respectively. For the roughly spherical analytes, the optimal tubule diameter is a little over twice the diameter of the molecule.

2. Molecular-Size-Based Selectivity

The data presented so far show a strong correlation between detection limit and the relative sizes of the nanotube and the analyte molecule (Figure 22). This indicates that this device should show molecular-size-based selectivity. This is not surprising given the transport studies discussed above. To explore size-based selectivity, a series of solutions was prepared containing decreasing concentrations of the analyte species but containing a constant (higher) concentration of an interfering species. The interfering species was smaller than the analyte species. The response of the nanotubule membrane (nanotube diameter = 2.8 nm) to these solutions was then measured starting from lowest to highest concentration of the analyte species.

The small pyridine molecule was used as the first interfering species. When present at a concentration of 10^{-4} M, pyridine offered very little interference for any of the analytes $Ru(bpy)_3^{2+}$, MV^{2+}, or quinine. The detection limits in the presence of 10^{-4} M pyridine were 10^{-10} M for $Ru(bpy)_3^{2+}$, 10^{-6} M for MV^{2+}, and 10^{-7} M for quinine, within an order of magnitude of the detection limit with no added interfering species (Table 2). Put another way, this device can detect 10^{-10} M $Ru(bpy)_3^{2+}$ in the presence of 6 orders of magnitude higher pyridine concentration.

A second set of experiments was done using the larger MV^{2+} as the interfering species. Now at low concentrations of analyte, there is a region where the device produces a constant response due to the constant concentration (10^{-4} M) of this interfering species; i.e., the much higher concentration of the MV^{2+} swamps the response of the device.[156] However, as the concentration of $Ru(bpy)_3^{2+}$ increases, there is a concentration range where the device responds to this analyte species without interference from the MV^{2+}. This concentration range begins at concentrations of $Ru(bpy)_3^{2+}$ above 10^{-8} M. That is, the size-based selectivity is such that the larger analyte species, $Ru(bpy)_3^{2+}$, can be detected down to 10^{-8} M in the presence of 4 orders of magnitude higher concentration of the smaller interfering species, MV^{2+}.

These data can be quantified by defining the selectivity coefficient $K_{bpy/MV}$ as the slope of the calibration curve for the analyte, $Ru(bpy)_3^{2+}$, divided by the slope for the interfering species, MV^{2+}. This analysis is somewhat problematic because the calibration curves are nonlinear and because the device is not very sensitive to MV^{2+}.[156] However, taking the data from the central part of the $Ru(bpy)_3^{2+}$ calibration curve gives a slope of ~400 A M^{-1}; dividing by the slope for the MV^{2+} data gives $K_{bpy/MV} = 4000$. These experiments show that, in agreement with the transport studies, the nanotubule membrane-based sensor can show excellent size-based selectivity. As discussed briefly above, selectivity could also be introduced by chemically derivatizing the inside walls of the nanotubules.[155,163]

V. Conclusions

In this review we have attempted to unify various apparently disparate sensing strategies. The unifying feature is the underlying measurement principle which entails occlusion of an aperture through which a current is passing by the analyte species. While we began with a classical and commercially available device, the review focused on two very recent manifestations of this sensing paradigm—the use of protein-based channels and nanotubule membranes for small molecule and ion sensing.

It is of interest to consider the relative advantages and disadvantages of these sensing strategies. The key advantages of the protein-based system are the capability to obtain an analyte signature by detecting single molecules as they enter and exit the protein channel and the ability to employ the power of protein engineering to create a variety of analyte binding sites in channels. The disadvantage of this approach is that the lipid bilayer membrane into which the channel is immobilized is fragile. By contrast, the key advantage of the nanotubule approach is that the membranes that contain them are mechanically strong. In addition, the inside diameter of the nanotubules can be controlled at will, as can the chemical environment within the nanotubules.

It seems reasonable to suggest that these two paradigms could be combined to yield a practical sensor that expresses the best features of both.

For example, apertures manufactured in inorganic substrates such as silicon, carbon, and gold might be used to support protein pores. Clearly, the nanoftubules described here, made by electroless plating of track-etched filters, would be candidates as apertures as they can be produced with appropriate dimensions. Further, the chemistry of the nanotubule surface might be tailored by modification with various thiols to make it more compatible with the protein,[155,163] and the protein could be reciprocally engineered for its new lodgings.

The future of stochastic sensing may lie in sensor elements where the advantages of structures such as the Au nanotubules and features from engineered proteins are combined into a single entity. In other words, after learning from experience with proteins, they might be abandoned altogether. For example, the adapters that have been used with protein pores might, after suitable modification, be inserted directly into the nanotubes. Alternatively, functional groups might be placed at the mouths of nanotubes or adapters covalently attached there. While these possibilities are attractive, it is likely that the versatility and precision of protein engineering will command the area for some time.

Finally, stochastic sensing need not be limited to electrical detection. Recent years have seen astonishing advances in single- molecule detection especially by optical and mechanical means and the principles discussed here might be implemented with the newly available tools. For example, progress in single-molecule fluorescence techniques has recently culminated in the ability to detect single enzyme turnovers.[15,171] Sensing with fluorescent receptors including channel proteins is an emerging possibility.[13] Force measurements have permitted examination of the unfolding of single protein domains,[4,172,173] and it should be possible to adapt this approach to reveal the kinetics of analyte binding to single receptor molecules.

VI. Acknowledgments

C.R.M. acknowledges support from the Office of Naval Research and the National Science Foundation. Work on stochastic sensing in the Bayley laboratory has been supported by DARPA, DOE, and ONR (H.B.). We thank Orit Braha and Liviu Movileanu for their comments on the manuscript. Both authors warmly thank the colleagues who have worked on the projects described in this review.

VII. References

(1) Lines, R. W. In "Particle Size Analysis," Stanley-Wood, N. G. and Lines, R. W., Eds.
(2) Kubitschek, H. E. In *Methods in Microbiology*; Norris, J. R., Ribbons, D. W., Eds.
(3) www.beckman.com/coulter/PC/SS000091.ASP.
(4) www.micromeritics.com/ps_elzone.html.
(5) Personal communication, Rick Shimkus, Micromeritics, Inc. July 27, 1999.
(6) Ramon, R.: Sawadogo, D.; Koko, F. S.; Noba, V.; Likikouet, R.; Gourvellec, G.; Viho, I.; Mandelbrot, L.; Dabis, F.; Ekra, C. W.; Msellati, P. *Trans. R. Soc. Trop. Med. Hyg.* **1999**, *93*, 419−422.
(7) Hwa, I. A. W.; Reimann, K.; Lim, P. K. C.; Lai, L. C. *Int. J. Mol. Med.* **1999**, *4*, 175−178.
(8) DeBlois, R. W.; Bean, C. P. *Rev. Sci. Instrum.* **1970**, *41*, 909−916.
(9) DeBlois, R. W.; Wesley, R. K. A. *J. Virol.* **1977**, *23*, 227−233.
(10) Fleischer, R. L.; Price, P. B.; Walker, R. M. *Nuclear Tracks in Solids*; University of California Press: Berkeley, CA, 1975.
(11) Sun, L.; Crooks, R. M. *Langmuir* **1999**, *15*, 738−741.
(12) Koch, M.; Evans, A. G. R.; Brunnschweiler, A. *J. Micromech. Microeng.* **1999**, *9*, 159−161.
(13) Weiss, S. *Science* **1999**, *283*, 1676−1683.
(14) Mehta, A. D.; Rief, M.; Spudich, J. A.; Smith, D. A.; Simmons, R. M. *Science* **1999**, *283*, 1689−1695.
(15) Xie, X. S.; Lu, H. P. *J. Biol. Chem.* **1999**, *274*, 15967−15970.
(16) Hille, B. *Ionic channels of excitable membranes*; Sinauer: Sunderland, MA, 1991.
(17) Mueller, P.; Rudin, D. O.; Tien, H. T.; Wescott, W. C. *Nature* **1962**, *194*, 979−980.
(18) Hladky, S. B.; Haydon, D. A. *Nature* **1970**, *225*, 451−453.
(19) Mueller, P.; Rudin, D. O. *J. Theor. Biol.* **1968**, *18*, 222−258.
(20) Bean, R. C.; Shepherd, W. C.; Chan, H.; Eichner, J. *J. Gen. Physiol.* **1969**, *53*, 741−757.
(21) Lindemann, B.; van Driessche, W. *Science* **1977**, *195*, 292−294.
(22) Neher, E.; Stevens, C. F. *Annu. Rev. Biophys. Bioeng.* **1977**, *6*, 345−381.
(23) Neher, E.; Sakmann, B. *Nature* **1976**, *260*, 779−802.
(24) Hamill, O. P.; Marty, A.; Neher, E.; Sakmann, B.; Sigworth, F. J. *Pflügers Arch.* **1981**, *391*, 85−100.
(25) Suarez-Isla, B. A.; Wan, K.; Lindstrom, J.; Montal, M. *Biochemistry* **1983**, *22*, 2319−2323.
(26) Coronado, R.; Latorre, R. *Biophys. J.* **1983**, *43*, 231−236.
(27) Hanke, W.; Schlue, W.-R. *Planar lipid bilayers*; Academic Press: London, 1993.
(28) Karlin, A.; Akabas, M. H. *Neuron* **1995**, *15*, 1227−1230.
(29) Armstrong, C. M.; Hille, B. *Neuron* **1998**, *20*, 371−380.
(30) Dingledine, R.; Borges, K.; Bowie, D.; Traynelis, S. F. *Pharmacol. Rev.* **1999**, *51*.
(31) Gouaux, E. *Curr. Opin. Struct. Biol.* **1997**, *7*, 566−573.
(32) Schulz, G. E. *Curr. Opin. Struct. Biol.* **1996**, *6*, 485−490.
(33) Pautsch, A.; Schulz, G. E. *Nature Struct. Biol.* **1998**, *5*, 1013−1017.
(34) Sansom, M. S. P. *Curr. Biol.* **1999**, *9*, R254−R257.
(35) Yellen, G. *Q. Rev. Biophys.* **1998**, *31*, 239−295.
(36) Locher, K. P.; Rees, B.; Koebnik, R.; Mitschler, A.; Moulinier, L.; Rosenbusch, J. P.; Moras, D. *Cell* **1998**, *95*, 771−778.
(37) Ferguson, A. D.; Hofmann, E.; Coulton, J. W.; Diedrichs, K.; Welte, W. *Science* **1998**, *282*, 2215−2220.
(38) Buchanan, S. K.; Smith, B. S.; Venkatramani, L.; Xia, D.; Esser, L.; Palni, M.; Chakraborty, R.; van der Helm, D.; Deisenhofer, J. *Nature Struct. Biol.* **1999**, *6*, 56−63.
(39) Woodhull, A. M. *J. Gen. Physiol.* **1973**, *61*, 687−708.
(40) Neher, E.; Steinbach, J. H. *J. Physiol.* **1978**, *277*, 153−176.
(41) Fukushima, Y. *J. Physiol.* **1982**, *331*, 311−331.
(42) Doyle, D. A.; Cabral, J. M.; Pfuetzner, R. A.; Kuo, A.; Gulbis, J. M.; Cohen, S. L.; Chait, B. T.; MacKinnon, R. *Science* **1998**, *280*, 69−77.
(43) Krasilnikov, O. V.; Sabirov, R. Z.; Ternovsky, V. I.; Merzliak, P. G.; Muratkhodjaev, J. N. *FEMS Microbiol. Immunol.* **1992**, *105*, 93−100.
(44) Vodyanoy, I.; Bezrukov, S. M. *Biophys. J.* **1992**, *62*, 10−11.
(45) Bezrukov, S. M.; Vodyanoy, I. *Biophys. J.* **1993**, *64*, 16−25.
(46) Zimmerberg, J.; Parsegian, V. A. *Nature* **1986**, *323*, 36−39.
(47) Nekolla, S.; Andersen, C.; Benz, R. *Biophys. J.* **1994**, *66*, 1388−1397.
(48) Andersen, C.; Jordy, M.; Benz, R. *J. Gen. Physiol.* **1995**, *105*, 385−401.
(49) Andersen, C.; Cseh, R.; Schülein, K.; Benz, R. *J. Membr. Biol.* **1998**, *164*, 263−274.
(50) DeFelice, L. J. *Introduction to membrane noise*; Plenum: New York, 1981.
(51) van Driessche, W. In *Noise and Impedance Analysis*; Schaffer, J. A., Geibisch, G., Kristensen, P., Ussing, H. H., Eds.; R. G. Landes Co.: 1994; pp 27−80.
(52) Heinemann, S.; Sigworth, F. J. *Biochim. Biophys. Acta* **1989**, *987*, 8−14.
(53) Bezrukov, S. M.; Kasianowicz, J. J. *Phys. Rev. Lett.* **1993**, *70*, 2352−2355.
(54) Rostovtseva, T. K.; Bezrukov, S. M. *Biophys. J.* **1998**, *74*, 2365−2373.
(55) Bezrukov, S. M.; Vodyanoy, I.; Parsegian, V. A. *Nature* **1994**, *370*, 279−281.
(56) Bezrukov, S. M.; Vodyanoy, I.; Brutyan, R. A.; Kasianowicz, J. J. *Macromolecules* **1996**, *29*, 8517−8522.
(57) Bezrukov, S. M.; Kasianowicz, J. J. *Eur. Biophys. J.* **1997**, *26*, 471−476.
(58) Arkin, I. T.; Adams, P. D.; MacKenzie, K. R.; Lemmon, M. A.; Brünger, A. T.; Engelman, D. M. *EMBO J.* **1994**, *13*, 4757−4764.
(59) Schirmer, T.; Keller, T. A.; Wang, Y.-F.; Rosenbusch, J. P. *Science* **1995**, *267*, 512−514.

(60) Dutzler, R.; Wang, Y.-F.; Rizkallah, P. J.; Rosenbusch, J. P.; Schirmer, T. *Structure* **1996**, *3*, 127−134.
(61) Gu, L.-Q.; Braha, O.; Conlan, S.; Cheley, S.; Bayley, H. *Nature* **1999**, *398*, 686−690.
(62) Kasianowicz, J. J.; Brandin, E.; Branton, D.; Deamer, D. W. *Proc. Natl. Acad. Sci. U.S.A.* **1996**, *93*, 13770−13773.
(63) Church, G.; Deamer, D. W.; Branton, D.; Baldarelli, R.; Kasianowicz, J. U.S. Patent 5,795,782, 1995; 1998.
(64) Alper, J. *Science* **1999**, *284*, 1754−1754.
(65) Lubensky, D. K.; Nelson, D. R. *Biophys. J.* **1999**, *77*, 1824−1838.
(66) Akeson, M.; Branton, D.; Kasianowicz, J. J.; Brandin, E.; Deamer, D. W. *Biophys. J.* **1999**, *77*, 3227−3233.
(67) Anderson, O. S. *Biophys. J.* **1999**, *77*, 2899−2901.
(68) Meller, A.; Nivon, L.; Brandin, E.; Golovchenko, J.; Branton, D. *Proc. Natl. Acad. Sci. U.S.A.* **2000**, *97*, 1079−1084.
(69) Merzlyak, P. G.; Yuldasheva, L. N.; Rodrigues, C. G.; Carneiro, C. M. M.; Krasilnikov, O. V.; Bezrukhov, S. M. *Biophys. J.* **1999**, *77*, 3023−3033.
(70) Hume, R. I.; Role, L. W.; Fischbach, G. D. *Nature* **1983**, *305*, 632−634.
(71) Young, S. H.; Poo, M. *Nature* **1983**, *305*, 634−637.
(72) Allen, T. G. J. *Trends Neurosci.* **1997**, *20*, 192−197.
(73) Kramer, R. H. *Neuron* **1990**, *4*, 335−341.
(74) Trivedi, B.; Kramer, R. H. *Neuron* **1998**, *21*, 895−906.
(75) Trivedi, B.; Vendiola, M. D.; Kramer, R. H. *Neuron*, in press.
(76) Shear, J. B.; Fishman, H. A.; Allbritton, N. L.; Garigan, D.; Zare, R. N.; Scheller, R. H. *Science* **1995**, *267*, 74−77.
(77) Orwar, O.; Jardemark, K.; Jacobson, I.; Moscho, A.; Fishman, H. A.; Scheller, R. H.; Zare, R. N. *Science* **1996**, *272*, 1779−1782.
(78) Jardemark, K.; Orwar, O.; Jacobson, I.; Moscho, A.; Zare, R. N. *Anal.Chem.* **1997**, *69*, 3427−3434.
(79) Fishman, H. A.; Greenwald, D. R.; Zare, R. N. *Annu. Rev. Biophys. Biomol. Struct.* **1998**, *27*, 165−198.
(80) Jardemark, K.; Farre, C.; Jacobsen, I.; Zare, R. N.; Orwar, O. *Anal.Chem.* **1998**, *70*, 2468−2474.
(81) Orwar, O.; Jardemark, K.; Farre, C.; Jacobson, I.; Moscho, A.; Shear, J. B.; Fishman, H. A.; Lillard, S. J.; Zare, R. N. *Methods Enzymol.* **1999**, *294*, 189−208.
(82) Bayley, H. *Curr. Opin. Biotechnol.* **1999**, *10*, 94−103.
(83) Cheley, S.; Braha, O.; Lu, X.; Conlan, S.; Bayley, H. *Protein Sci.* **1999**, *8*, 1257−1267.
(84) Fleming, K. G.; Ackerman, A. L.; Engelman, D. M. *J. Mol. Biol.* **1997**, *272*, 266−275.
(85) MacKenzie, K. R.; Engelman, D. M. *Proc. Natl. Acad. Sci. U.S.A.* **1998**, *95*, 3583−3590.
(86) Benson, D. E.; Wisz, M. S.; Hellinga, H. W. *Curr. Opin. Biotechnol.* **1998**, *9*, 370−376.
(87) Distefano, M. D.; Kuang, H.; Qi, D.; Mazhary, A. *Curr. Opin. Struct. Biol.* **1998**, *8*, 459−465.
(88) Preston, G. M.; Sup Jung, J.; Guggino, W. B.; Agre, P. *J. Biol. Chem.* **1993**, *268*, 17−20.
(89) Lü, Q.; Miller, C. *Science* **1995**, *268*, 304−307.
(90) Elling, C. E.; Nielsen, S. M.; Schwartz, T. W. *Nature* **1995**, *374*, 74−77.
(91) Elling, C. E.; Thirstrup, K.; Nielsen, S. M.; Hjorth, S. A.; Schwartz, T. W. *Fold. Des.* **1997**, *2*, S76−S80.
(92) Braha, O.; Walker, B.; Cheley, S.; Kasianowicz, J. J.; Song, L.; Gouaux, J. E.; Bayley, H. *Chem. Biol.* **1997**, *4*, 497−505.
(93) Forman, S. A.; Miller, K. W.; Yellen, G. *Mol. Pharmacol.* **1995**, *48*, 574−581.
(94) Forman, S. A. *Biophys. J.* **1997**, *72*, 2170−2179.
(95) Baltzer, L. *Curr. Opin. Struct. Biol.* **1998**, *8*, 466−470.
(96) Corey, D. R.; Schultz, P. G. *Science* **1987**, *238*, 1401−1403.
(97) Corey, D. R.; Pei, D.; Schultz, P. G. *Biochemistry* **1989**, *28*, 8277−8286.
(98) Zuckermann, R. N.; Schultz, P. G. *Proc. Natl. Acad. Sci. U.S.A.* **1989**, *86*, 1766−1770.
(99) Pei, D.; Corey, D. R.; Schultz, P. G. *Proc. Natl. Acad. Sci. U.S.A.* **1990**, *87*, 9858−9862.
(100) Hamachi, I.; Nagase, T.; Tajiri, Y.; Shinkai, S. *Bioconjugate Chem.* **1997**, *8*, 862−868.
(101) Lehn, J.-M. *Supramolecular chemistry: concepts and perspectives*; VCH: Weinheim, 1995.
(102) *Comprehensive supramolecular chemistry*; Lehn, J.-M., Atwood, J. L., Davies, J. E. D., Macnicol, D. D., Vögtle, F., Eds.; 1997.
(103) Nowak, M. W.; Kearney, P. C.; Sampson, J. R.; Saks, M. E.; Labarca, C. G.; Silverman, S. K.; Zhong, W.; Thorson, J.; Abelson, J. N.; Davidson, N.; Schultz, P. G.; Dougherty, D. A.; Lester, H. A. *Science* **1995**, *268*, 439−442.
(104) Kearney, P. C.; Zhang, H.; Zhong, W.; Dougherty, D. A.; Lester, H. A. *Neuron* **1996**, *17*, 1221−1229.
(105) Gallivan, J. P.; Lester, H. A.; Dougherty, D. A. *Chem. Biol.* **1997**, *4*, 739−749.
(106) England, P. M.; Lester, H. A.; Davidson, N.; Dougherty, D. A. *Proc. Natl. Acad. Sci. U.S.A.* **1997**, *94*, 11025−11030.
(107) Miller, J. C.; Silverman, S. K.; England, P. M.; Dougherty, D. A.; Lester, H. A. *Neuron* **1998**, *20*, 619−624.
(108) England, P. M.; Zhang, Y.; Dougherty, D. A.; Lester, H. A. *Cell* **1999**, *96*, 89−98.
(109) Liman, E. R.; Tytgat, J.; Hess, P. *Neuron* **1992**, *9*, 861−871.
(110) Yang, J.; Jan, Y. N.; Jan, L. Y. *Neuron* **1995**, *15*, 1441−1447.
(111) Gouaux, J. E.; Braha, O.; Hobaugh, M. R.; Song, L.; Cheley, S.; Shustak, C.; Bayley, H. *Proc. Natl. Acad. Sci. U.S.A.* **1994**, *91*, 12828−12831.
(112) Åkerfeldt, K. S.; Lear, J. D.; Wasserman, Z. R.; Chung, L. A.; DeGrado, W. F. *Acc. Chem. Res.* **1993**, *26*, 191−197.
(113) Montal, M. *Curr. Opin. Struct. Biol.* **1995**, *5*, 501−506.
(114) Lear, J. D.; Schneider, J. P.; Kienker, P. K.; DeGrado, W. F. *J. Am. Chem. Soc.* **1997**, *119*, 3212−3217.
(115) Montal, M. O.; Iwamoto, T.; Tomich, J. M.; Montal, M. *FEBS Lett.* **1993**, *320*, 261−266.
(116) Pawlak, M.; Meseth, U.; Dhanapal, B.; Mutter, M.; Vogel, H. *Protein Sci.* **1994**, *3*, 1788−1805.
(117) Futaki, S.; Aoki, M.; Fukuda, M.; Kondo, F.; Niwa, M.; Kitagawa, K.; Nakaya, Y. *Tetrahedron Lett.* **1997**, *38*, 7071−7074.
(118) Hartgerink, J. D.; Clark, T. D.; Ghadiri, M. R. *Chem. Eur. J.* **1998**, *4*, 1367−1372.
(119) Ghadiri, M. R.; Granja, J. R.; Buehler, L. K. *Nature* **1994**, *369*, 301−304.
(120) Clark, T. D.; Buehler, L. K.; Ghadiri, M. R. *J. Am. Chem. Soc.* **1998**, *120*, 651−656.
(121) Smithrud, D. B.; Benkovic, S. J. *Curr. Opin. Biotechnol.* **1997**, *8*, 459−466.
(122) Wade, H.; Scanlan, T. S. *Annu. Rev. Biophys. Biomol. Struct.* **1997**, *26*, 461−493.
(123) Wentworth, P.; Janda, K. D. *Curr. Opin. Chem. Biol.* **1998**, *2*, 138−144.
(124) Kasianowicz, J. J.; Burden, D. L.; Han, L. C.; Cheley, S.; Bayley, H. *Biophys. J.* **1999**, *76*, 837−845.
(125) Bhakdi, S.; Bayley, H.; Valeva, A.; Walev, I.; Walker, B.; Weller, U.; Kehoe, M.; Palmer, M. *Arch. Microbiol.* **1996**, *165*, 73−79.
(126) Gouaux, E. *J. Struct. Biol.* **1998**, *121*, 110−122.
(127) Song, L.; Hobaugh, M. R.; Shustak, C.; Cheley, S.; Bayley, H.; Gouaux, J. E. *Science* **1996**, *274*, 1859−1865.
(128) Füssle, R.; Bhakdi, S.; Sziegoleit, A.; Tranum-Jensen, J.; Kranz, T.; Wellensiek, H.-J. *J. Cell Biol.* **1981**, *91*, 83−94.
(129) Bhakdi, S.; Muhly, M.; Füssle, R. *Infect. Immunol.* **1984**, *46*, 318−323.
(130) Olson, R.; Nariya, H.; Yokota, K.; Kamio, Y.; Gouaux, E. *Nature Struct. Biol.* **1999**, *6*, 134−140.
(131) Walker, B.; Bayley, H. *Protein Eng.* **1995**, *8*, 491−495.
(132) Valeva, A.; Weisser, A.; Walker, B.; Kehoe, M.; Bayley, H.; Bhakdi, S.; Palmer, M. *EMBO J.* **1996**, *15*, 1857−1864.
(133) Walker, B. J.; Krishnasastry, M.; Zorn, L.; Kasianowicz, J. J.; Bayley, H. *J. Biol. Chem.* **1992**, *267*, 10902−10909.
(134) Menestrina, G. *J. Membr. Biol.* **1986**, *90*, 177−190.
(135) Walker, B.; Kasianowicz, J.; Krishnasastry, M.; Bayley, H. *Protein Eng.* **1994**, *7*, 655−662.
(136) Pédelacq, J.-D.; Maveyraud, L.; Prévost, G.; Baba-Moussa, L.; González, A.; Courcelle, E.; Shepard, W.; Monteil, H.; Samama, J.-P.; Mourey, L. *Structure* **1999**, *7*, 277−288.
(137) Walker, B.; Braha, O.; Cheley, S.; Bayley, H. *Chem. Biol.* **1995**, *2*, 99−105.
(138) D'Souza, V. T.; Lipkowitz, K. B. *Chem. Rev.* **1998**, *98* (5), special issue.
(139) Rekharsky, M. V.; Inoue, Y. *Chem. Rev.* **1998**, *98*, 1875−1917.
(140) Chang, G.; Spencer, R. H.; Lee, A. T.; Barclay, M. T.; Rees, D. C. *Science* **1998**, *282*, 2220−2226.
(141) Dahiyat, B. I.; Mayo, S. L. *Science* **1997**, *278*, 82−87.
(142) DeGrado, W. F. *Science* **1997**, *278*, 80−81.
(143) Dieckmann, G. R.; DeGrado, W. F. *Curr. Opin. Struct. Biol.* **1997**, *7*, 486-494.
(144) Griffin, B. A.; Adams, S. R.; Tsien, R. Y. *Science* **1998**, *281*, 269−272.
(145) Sackmann, E. *Science* **1996**, *271*, 43−48.
(146) Heyse, S.; Stora, T.; Schmid, E.; Lakey, J. H.; Vogel, H. *Biochim. Biophys. Acta* **1998**, *1376*, 319−338.
(147) Raguse, B.; Braach-Maksvytis, V.; Cornell, B. A.; King, L. G.; Osman, P. D. J.; Pace, R. J.; Wieczorek, L. *Langmuir* **1998**, *14*, 648−659.
(148) Gritsch, S.; Nollert, P.; Jähnig, F.; Sackmann, E. *Langmuir* **1998**, *14*, 3118−3125.
(149) Cornell, B. A.; Braach-Maksvytis, V. L. B.; King, L. G.; Osman, P. D. J.; Raguse, B.; Wieczorek, L.; Pace, R. J. *Nature* **1997**, *387*, 580−583.
(150) Stora, T.; Lakey, J. H.; Vogel, H. *Angew. Chem., Int. Ed. Engl.* **1999**, *38*, 389−392.
(151) Schuster, B.; Pum, D.; Braha, O.; Bayley, H.; Sleytr, U. B. *Biochim. Biophys. Acta* **1998**, *1370*, 280−288.
(152) Schuster, B.; Pum, D.; Sleytr, U. B. *Biochim. Biophys. Acta* **1998**, *1369*, 51−60.
(153) Nishizawa, M.; Menon, V. P.; Martin, C. R. *Science* **1995**, *268*, 700−702.
(154) Jirage, K. B.; Hulteen, J. C.; Martin, C. R. *Science* **1997**, *278*, 655−658.
(155) Hulteen, J. C.; Jirage, K. B.; Martin, C. R. *J. Am. Chem. Soc.* **1998**, *120*, 6603−6605.
(156) Kobayashi, Y.; Martin, C. R. *Anal. Chem.* **1999**, *71*, 3665−3672.

(157) Kobayashi, Y.; Martin, C. R. *J. Electroanal. Chem.* **1997**, *431*, 29−33.
(158) Hulteen, J. C.; Martin, C. R. *J. Mater. Chem.* **1997**, *7*, 1075−1087.
(159) Martin, C. R. *Science* **1994**, *266*, 1961−1966.
(160) Menon, V. P.; Martin, C. R. *Anal. Chem.* **1995**, *67*, 1920−1928.
(161) Che, G.; Lakshmi, B. B.; Fisher, E. R.; Martin, C. R. *Nature* **1998**, *398*, 346−349.
(162) Che, G.; Lakshmi, B. B.; Martin, C. R.; Fisher, E. R. *Langmuir* **1999**, *15*, 750−758.
(163) Jirage, K. B.; Hulteen, J. C.; Martin, C. R. *Anal. Chem.* **1999**, *71*, 4913−4918.
(164) Petzny, W. J.; Quinn, J. A. *Science* **1969**, *166*, 751.
(165) Prat, Z.: Tricot, Y.-M.; Rubinstein, I. *J. Electroanal. Chem.* **1991**, *315*, 225.
(166) Martin, C. R.; Rubinstein, I.; Bard, A. J. *J. Electroanal. Chem.* **1983**, *115*, 267.
(167) Deen, V. M. *AICHEJ* **1987**, *33*, 14091425.
(168) Kathawalla, I. A.; Anderson, J. L.; Lindsey, J. S. *Macromolecules* **1989**, *22*, 1215−1219.
(169) Nitsche, J. M.; Balgi, G. *Ind. Eng. Chem. Res.* **1994**, *33*, 2242−2247.
(170) Rostovtseva, T. K. *J. Membr. Biol.* **1996**, *151*, 29.
(171) Lu, H. P.; Xun, L.; Xie, X. S. *Science* **1998**, *282*, 1877−1882.
(172) Rief, M.; Gautel, M.; Oesterhelt, F.; Fernandez, J. M.; Gaub, H. E. *Science* **1997**, *276*, 1109−1112.
(173) Oberhauser, A. F.; Marszalek, P. E.; Erickson, H. P.; Fernandez, J. M. *Nature* **1998**, *393*, 181−185.

CR980099G